arXiv:1602.02381v1 [math.AP] 7 Feb 2016

LOCAL STRUCTURE OF SINGULAR PROFILES FOR A DERIVATIVE NONLINEAR SCHRÖDINGER EQUATION

YURI CHER, GIDEON SIMPSON, AND CATHERINE SULEM

Abstract. The Derivative Nonlinear Schrödinger equation is an L^2-critical nonlinear dispersive equation model for Alfvén waves in space plasmas. Recent numerical studies [12] on an L^2-supercritical extension of this equation provide evidence of finite time singularities. Near the singular point, the solution is described by a universal profile that solves a nonlinear elliptic eigenvalue problem depending only on the strength of the nonlinearity. In the present work, we describe the deformation of the profile and its parameters near criticality, combining asymptotic analysis and numerical simulations.

1. Introduction

The derivative nonlinear Schrödinger (DNLS) equation

$$\begin{cases} iu_t + u_{xx} + i\left(|u|^2 u\right)_x = 0, \quad x \in \mathbb{R} \\ u(x,0) = u_0(x). \end{cases} \tag{1.1}$$

is a canonical equation arising from the Hall-Magnetohydrodynamics equations. It appears in the context of Alfvén waves propagating along an ambient unidirectional magnetic field in a long wavelength regime [20]. More recently, it was used to model rogue waves and plasma turbulence [18]. Under the gauge transformation,

$$\psi(x,t) = u(x,t) \exp\left\{ \frac{i}{2} \int_{-\infty}^{x} |u(y,t)|^2 dy \right\}, \tag{1.2}$$

(1.1) becomes

$$i\psi_t + \psi_{xx} + i|\psi|^2 \psi_x = 0. \tag{1.3}$$

Eq. (1.3) has appeared as a model for ultrashort optical pulses, [2, 16, 21].

Date: February 9, 2016.

1991 *Mathematics Subject Classification.* 35Q55, 37K40, 35Q51, 65M60.

Key words and phrases. Derivative Nonlinear Schrödinger Equation, Blowing-up Solutions, Boundary-value Problems.

G.S. is partially supported by NSF through grant number DMS-1409018. Work reported here was run on hardware supported by Drexel's University Research Computing Facility.

C.S. is partially supported by NSERC through grant number 46179–13.

Solutions to the DNLS equation exist locally in time in $H^1(\mathbb{R})$ and they can be extended for all time if the initial conditions are sufficiently small in L^2, namely $\|u_0\|_2 < \sqrt{2\pi}$ [8, 9]. The global in time result relies on two invariants of the equation,

$$\text{Mass:} \quad M[u] \equiv \int |u|^2 \; dx, \tag{1.4}$$

$$\text{Hamiltonian:} \quad H[u] \equiv \int \left(|u_x|^2 + \tfrac{3}{2}\Im(|u|^2 u\bar{u}_x) + \tfrac{1}{6}|u|^6 \right) dx \tag{1.5}$$

and the sharp constant in a Gagliardo-Nirenberg inequality. Very recently, Wu [22] showed that the upper bound on the L^2-norm of the initial conditions can be increased to $\|u_0\|_2 < \sqrt{4\pi}$ using the conservation of momentum

$$\text{Momentum:} \quad I[u] \equiv \int \left(\Im(\bar{u}u_x) - \tfrac{1}{2}|u|^4 \right) dx \tag{1.6}$$

and a different Gagliardo-Nirenberg inequality. As discussed below, DNLS has a two-parameter family of solitary waves that decay exponentially fast at infinity (bright solitons) as well as algebraic solitons (lumps). It is interesting to notice that $\sqrt{4\pi}$ is the L^2-norm of the lump soliton (see (2.4) with $\sigma = 1$). Furthermore, DNLS is completely integrable via the inverse scattering transform [10] and has an infinite number of conserved quantities. Recent works using the inverse scattering method provide global solutions for initial conditions in a spectrally determined (open) subset of weighted Sobolev spaces containing a neighborhood of zero, [11,17]. Global well-posedness for large data remains an open problem.

Equation (1.3), along with (1.1), is invariant to the scaling transformation $\psi \mapsto \psi_\lambda = \lambda^{-\frac{1}{2}}\psi(\lambda^{-1}x, \lambda^{-2}t)$. It is L^2-critical in the sense that $\|\psi_\lambda\|_{L^2} = \|\psi\|_{L^2}$ and has the same scaling properties as the focusing nonlinear Schrödinger equation,

$$iu_t + \Delta u + |u|^{2\sigma} u = 0, \quad u : (x,t) \in \mathbb{R}^d \times \mathbb{R} \to \mathbb{C}, \tag{1.7}$$

with $d\sigma = 2$. However, it has very different structural properties, such as the aforementioned integrability. In contrast, it is well known that for the L^2-critical and supercritical NLS equations ($d\sigma \geq 2$), blowup occurs for initial conditions with L^2-norm exceeding that of the ground state.

In the context of dispersive equations, the comparative study of equations with critical and supercritical nonlinearities has been very fruitful, [15, 20]. From this perspective, and to gain additional insight into the properties of solutions to the DNLS equations, a generalization of (1.3) was introduced,

$$i\psi_t + \psi_{xx} + i|\psi|^{2\sigma}\psi_x = 0, \tag{1.8}$$

that we will refer to as "gDNLS", [12, 13]. If $\sigma > 1$, the gDNLS equation is L^2-supercritical. Recent work by Hayashi and Ozawa [7] shows that it is locally well-posed in H^1 and globally well-posed if the initial conditions are small enough; see Ambrose and Simpson for related results on the periodic problem, [1]. Numerical simulations performed in [12] strongly indicate that

(1.8) may present finite time singularities when $\sigma > 1$. More specifically, near the singular point, (x^*, t^*), the solution is locally approximated by

$$\psi(x,t) \approx \left(\frac{1}{2a(t^*-t)}\right)^{1/4\sigma} Q\left(\frac{x-x^*}{\sqrt{2a(t^*-t)}} + \frac{b}{a}\right) e^{i\left(\theta + \frac{1}{2a}\ln\frac{t^*}{t^*-t}\right)}. \tag{1.9}$$

The blow-up profile Q is a complex-valued function solving the nonlinear eigenvalue problem

$$Q_{\xi\xi} - Q + ia\left(\tfrac{1}{2\sigma}Q + \xi Q_\xi\right) - ibQ_\xi + i|Q|^{2\sigma}Q_\xi = 0. \tag{1.10}$$

The coefficient b can be changed, or even eliminated by translating the independent variable (as long as $a \neq 0$). It was observed numerically that the amplitude $|Q|$ of the profile has only one maximum. In this work, we will choose the coefficient b so that $\max|Q|$ is at the origin. The coefficients a, b, and the function Q all depend on σ, but were observed in the simulations to be universal (up to simple scalings), in the sense that the same values emerged, regardless of the initial conditions, for the time dependent problem.

The local structure of ψ, near the singularity, can be extracted using time dependent rescaling. First, we note that gDNLS is invariant under the transformation $\psi \mapsto \psi_\lambda = \lambda^{-\frac{1}{2\sigma}}\psi(\lambda^{-1}x, \lambda^{-2}t)$. This motivates the introduction of the scaled dependent and independent variables:

$$\psi(x,t) = \lambda(t)^{-\frac{1}{2\sigma}} v(\xi,\tau), \quad \xi = \frac{x - x_0(t)}{\lambda(t)}, \quad \tau = \int_0^t \frac{dt'}{\lambda^2(t')}. \tag{1.11}$$

The scaling factor $\lambda(t)$ is chosen to be proportional to $\|\psi_x\|_{L^2}^{-q}$, $q = 2\sigma/(\sigma+1)$, while the shift $x_0(t)$ is used to keep the bulk of the solution at the origin. The rescaled function v satisfies

$$\begin{cases} iv_\tau + v_{\xi\xi} + i\alpha(\tau)\left(\frac{v}{2\sigma} + \xi v_\xi\right) - i\beta(\tau)v_\xi + i|v|^{2\sigma}v_\xi = 0 \\ \alpha = -\lambda\frac{d\lambda}{dt}, \quad \beta = \lambda\frac{dx_0}{dt}. \end{cases} \tag{1.12}$$

For large τ, it was observed that $v \sim e^{iC\tau}Q(\xi)$ and the parameters $\alpha(\tau)$, $\beta(\tau)$ tend to constant values independent of the initial conditions. Substituting in $v \sim e^{iC\tau}Q(\xi)$, canceling out the time harmonic piece, and applying a simple rescaling turns (1.12) into (1.10). Under the transformation (1.11) the conserved quantities scale like

$$M(\psi) = \lambda^{1-\frac{1}{\sigma}}M(v), \quad H(\psi) = \lambda^{-1-\frac{1}{\sigma}}H(v), \quad I(\psi) = \lambda^{-\frac{1}{\sigma}}I(v).$$

In particular, since $\lambda \to 0$ as $\tau \to \infty$, we have that $M(Q) = \infty$ while $I(Q) = H(Q) = 0$. The blow-up profile equation is reminiscent of the profile describing the singularity structure of radially symmetric L^2-supercritical NLS equations (1.7), with $\sigma d > 2$ satisfying

$$S_{\xi\xi} + \tfrac{d-1}{\xi}S_\xi - S + ia\left(\tfrac{1}{\sigma}S + \xi S_\xi\right) + |S|^{2\sigma}S = 0, \quad \xi > 0, \tag{1.13}$$

derived in [14] and studied in [6]. An asymptotic analysis near the critical value $\sigma d \to 2$ [20] provides the behavior of the parameter a

$$\sigma d - 2 \propto a^{-1} e^{-\frac{\pi}{a}}, \quad \sigma d \to 2, \tag{1.14}$$

and the profile Q is asymptotically close to NLS ground state. This approach was key to predicting the generic blowup of solutions to critical NLS and its $\log - \log$ correction.

The simulations performed in [12] suggested that, as the nonlinearity $\sigma \to 1$, the coefficients a and b, viewed as functions of σ, behave as $a \to 0$ and $b \to b_0 > 0$. In the present work, we perform a detailed asymptotic study complemented by numerical results to describe the deformation of profile Q and the behaviour of the parameters $a(\sigma)$, $b(\sigma)$ in the $\sigma \to 1$ limit. We find that

$$Q(\xi) \sim L(\xi) \exp\left\{-i\left(\frac{a\xi^2}{4} - \frac{b\xi}{2} + \frac{1}{4}\int_0^\xi |Q|^2\right)\right\} \tag{1.15}$$

where $L(\xi) = \sqrt{\frac{8}{1+4\xi^2}}$ is the algebraic soliton of the DNLS solving

$$L_{\xi\xi} - L^3 + \tfrac{3}{16}L^5 = 0. \tag{1.16}$$

The parameters $a(\sigma)$ and $b(\sigma)$ behave like power laws of $(\sigma - 1)$, namely:

$$a \propto (\sigma - 1)^{\gamma_a}, \ \gamma_a \approx 3.2, \tag{1.17a}$$

$$2 - b \propto (\sigma - 1)^{\gamma_b}, \ \gamma_b = 2. \tag{1.17b}$$

Our paper is organized as follows. In Section 2, we describe basic properties of the profile Q solution of (1.10). In Section 3, we present numerical simulations of (1.10). Motivated by these calculations, we analyze the deformation of the profile as $\sigma \to 1$ and connect the behavior of Q at $\pm\infty$ using asymptotic methods in Section 4. We complement it by a careful analysis of the numerical data to predict relations between the parameters a and b and σ in the limit $\sigma \to 1$. In Section 5, we impose the vanishing momentum condition to extract another relation between the parameters. Concluding remarks are presented in Section 6. Finally, in Appendix A, we give the proof of Proposition 2.3 on the behavior of the profile $Q(\xi)$ for large ξ, and in Appendix B, we provide details of the numerical methods, in particular how we deal with solutions that decay slowly at infinity.

2. Preliminary Results

We recall basic properties of solutions to the profile equation (1.10), give a preliminary discussion on the relation between them and soliton solutions to the gDNLS equation.

2.1. **gDNLS Soliton Solutions.** The gDNLS equation (1.8) has a two-parameter family of soliton solutions in the form

$$\psi_{\omega,c}(x,t) = R_{\omega,c}(x-ct)\exp\left\{i\Big(\omega t + \frac{c}{2}(x-ct) - \frac{1}{2\sigma+2}\int_{-\infty}^{x-ct} R_{\omega,c}^{2\sigma}\Big)\right\},$$

where $R_{\omega,c}$, satisifies

$$\partial_{\xi\xi}R_{\omega,c} - \left(\omega - \tfrac{c^2}{4}\right)R_{\omega,c} - \frac{c}{2}\,|R_{\omega,c}|^{2\sigma}\,R_{\omega,c} + \tfrac{2\sigma+1}{(2\sigma+2)^2}\,|R_{\omega,c}|^{4\sigma}\,R_{\omega,c} = 0, \tag{2.1}$$

subject to the boundary conditions $R_{\omega,c} \to 0$ as $\xi \to \pm\infty$. Eq. (2.1) has smooth, real valued, solutions expressed in terms of hyperbolic functions for all c and $\omega > c^2/4$. Without loss of generality, we fix $\omega = 1$, denote $c = b$, and suppress the subscripts. The equation for R is then

$$R_{\xi\xi} - \left(1 - \tfrac{b^2}{4}\right)R - \frac{b}{2}R^{2\sigma+1} + \tfrac{2\sigma+1}{(2\sigma+2)^2}R^{4\sigma+1} = 0. \tag{2.2}$$

For $|b| < 2$, the solutions are smooth and exponentially decaying,

$$R = B_\sigma \equiv \left(\frac{(\sigma+1)(4-b^2)}{2(\cosh(\sigma\sqrt{4-b^2}\xi) - \frac{b}{2})}\right)^{\frac{1}{2\sigma}}. \tag{2.3}$$

We refer to these as "bright" soliton solutions. In the limit $b \nearrow 2$, another solution emerges, the algebraic "lump" soliton

$$R = L_\sigma \equiv \left(\frac{4(\sigma+1)}{1+4\sigma^2\xi^2}\right)^{\frac{1}{2\sigma}}. \tag{2.4}$$

Both types of solitons play roles in our study of the blowup profile.

2.2. **Properties of the blow-up profile.** We recall properties of solutions to the profile equation (1.10). Details of the proofs can be found in [12].

Proposition 2.1. *Let Q be a classical bounded solution of* (1.10) *with $a > 0$, such that $Q_\xi \in L^2$ and $Q \in L^{4\sigma+2}$. Then its energy and momentum vanish:*

$$H(Q) \equiv \int_{\mathbb{R}} \Big(|Q_\xi|^2 + \tfrac{1}{\sigma+1}|Q|^{2\sigma}\Im(\bar{Q}Q_\xi)\Big)\,d\xi = 0 \tag{2.5a}$$

$$I(Q) \equiv \Im\int_{\mathbb{R}} \bar{Q}Q_\xi d\xi = 0. \tag{2.5b}$$

Proof. We multiply (1.10) by $\bar{Q}_{\xi\xi}$ and integrate the imaginary part of the equation to get

$$-a\left(\tfrac{\sigma+1}{2\sigma}\right)\int |Q_\xi|^2 + \int |Q|^{2\sigma}\Re(Q_{\xi\xi}\bar{Q}_\xi) = 0.$$

In the second term we replace $Q_{\xi\xi}$ using (1.10) leading to

$$\int |Q|^{2\sigma}\Re(Q_{\xi\xi}\bar{Q}_\xi) = -\frac{a}{2\sigma}\int |Q|^{2\sigma}\Im(\bar{Q}Q_\xi).$$

If $a \neq 0$ the identity (2.5a) follows.

Similarly, multiplying (1.10) by $\bar{Q}_\xi$ and taking the real part of the equation gives

$$\partial_\xi |Q_\xi|^2 + \partial_\xi |Q|^2 + \tfrac{a}{\sigma} \Im \left(\bar{Q} Q_\xi \right) = 0.$$

If $a > 0$, integrating over the real line gives (2.5b). □

Proposition 2.2. *If Q is a solution of (1.10) with $a > 0$ and $\sigma > 1$, and $Q \in H^1 \bigcap L^{2\sigma+2}$, then $Q \equiv 0$.*

Consequently, there are no nontrivial solutions that belong to $H^1 \cap L^{2\sigma+2}$. The behaviour of solutions to (1.10) as $\xi \to \pm\infty$ can be written as $Q = A_\pm Q_1 + B_\pm Q_2$ where Q_1 and Q_2 behave at leading order as $Q_1 \approx |\xi|^{-\frac{1}{2\sigma} - \frac{i}{a}}$ and $Q_2 \approx e^{-i\frac{a\xi^2}{2}} |\xi|^{1 - \frac{1}{2\sigma} + \frac{i}{a}}$. Note that for $\sigma > 1$, $a > 0$, $Q_1 \notin L^2$ and $Q_{2_\xi} \notin L^2$. We are interested in solutions of (1.10) with $B_\pm = 0$, *i.e.* those that behave like Q_1 as $|\xi| \to \infty$. These are the types of profiles which correspond to finite energy solutions to the gDNLS equation.

Proposition 2.3. *The large ξ behaviour of zero-energy solutions to* (1.10) *is*

$$Q = A_\pm Q_1 \approx A_\pm |\xi|^{-\frac{1}{2\sigma}} \left(1 \pm \frac{b}{2a\sigma|\xi|} \right) e^{-\frac{i}{a}\left(\ln|\xi| \pm \frac{b}{a|\xi|} \right)}, \quad \xi \to \pm\infty. \tag{2.6}$$

This result is a slight refinement of Proposition 4.1 of [12]. A proof is presented in Appendix A.

2.3. **Phase–Amplitude Decomposition.** To further analyse the profile equation, we introduce the function P defined by

$$Q = P \exp\left\{ -i \left(\frac{a\xi^2}{4} - \frac{b\xi}{2} + \frac{1}{2\sigma+2} \int_0^\xi |Q|^{2\sigma} \right) \right\}. \tag{2.7}$$

We have extracted a portion of the phase corresponding to the gDNLS soliton as well as a quadratic part as is often the case in the study of NLS equations. P is complex valued and solves

$$\begin{aligned} &P_{\xi\xi} + \left(\tfrac{1}{4}(a\xi - b)^2 - 1 \right) P - i\tfrac{a(\sigma-1)}{2\sigma} P + \tfrac{1}{2}(a\xi - b)|P|^{2\sigma} P \\ &\quad + \tfrac{2\sigma+1}{(2\sigma+2)^2} |P|^{4\sigma} P - \tfrac{\sigma}{\sigma+1} |P|^{2(\sigma-1)} \Im(\bar{P} P_\xi) P = 0. \end{aligned} \tag{2.8}$$

When $a = 0$, we can also assume that P is real valued, and (2.8) becomes (2.2). This illustrates the connection between the blowup profile and the soliton. When $a \neq 0$, the function P is complex valued and it is useful to decompose it into a real valued amplitude and phase. Setting $P = Ae^{i\phi}$, we observe that only the derivative of the phase appears in the equations. Therefore, letting $\psi = \phi_\xi$, we have the system:

$$\begin{aligned} &A_{\xi\xi} + \left(\tfrac{1}{4}(a\xi - b)^2 - 1 - \psi^2 \right) A + \left(\tfrac{1}{2}(a\xi - b) - \tfrac{\sigma}{\sigma+1}\psi \right) A^{2\sigma+1} \\ &\qquad + \tfrac{2\sigma+1}{(2\sigma+2)^2} A^{4\sigma+1} = 0, \end{aligned} \tag{2.9a}$$

$$\psi_\xi A + 2\psi A_\xi = \tfrac{a(\sigma-1)}{2\sigma} A. \tag{2.9b}$$

(2.9b) can be written as

$$\left(A^2\psi\right)_\xi = \tfrac{a(\sigma-1)}{2\sigma}A^2$$

leading to an expression of ψ in terms of A^2

$$\psi(\xi) = \frac{\psi(0)A^2(0)}{A^2(\xi)} + \frac{a(\sigma-1)}{2\sigma A^2(\xi)}\int_0^\xi A^2(\eta)d\eta. \tag{2.10}$$

Alternatively, writing (2.9b) as

$$\frac{\left(A^2\psi\right)_\xi}{A^2\psi} = \frac{a(\sigma-1)}{2\sigma\psi},$$

we have the relation

$$A^2(\xi) = \frac{C^2}{|\psi|}\exp\left\{\frac{a(\sigma-1)}{2\sigma}\int_{\xi_0}^\xi \frac{d\eta}{\psi(\eta)}\right\}. \tag{2.11}$$

$C^2 = A^2(\xi_0)|\psi(\xi_0)|$ is a constant of integration. In both cases, the unknown constants depend on σ. For reference, the derivatives of the phase of Q and that of P are related as

$$\theta_\xi = \psi - \frac{a\xi - b}{2} - \frac{1}{2\sigma+2}|Q|^{2\sigma} \tag{2.12}$$

3. Numerical simulation of the profile equation

Here, we briefly summarize our approach to solving (1.10) and make some preliminary obsevations on the profiles.

3.1. **Solvability and Boundary Conditions.** To solve for the profile Q, and the parameters a and b, it is necessary to impose a sufficient number of boundary conditions and solvability conditions. These are as follows : (i) Since the profile equation is invariant under multiplication by a constant phase, we assume $Q(0) \in \mathbb{R}$; (ii) Proposition 2.3 gives a far-field, asymptotically linear approximation of Q which will be used to construct Robin boundary conditions, eliminating the constants A_+ and A_-; (iii) The parameter b can be changed by a translation in ξ. Under the assumption that the profile has a unimodal amplitude, which is consistent with numerical observations, we assume that the maximum of the amplitude occurs at the origin. We express this internal boundary condition as $|Q|_\xi(0) = 0$.

Preliminary numerical simulations of (1.10) subject to above boundary conditions were performed in [12]. It was observed that the amplitude A of Q is highly asymmetric and that the parameter a tends rapidly to zero as $\sigma \to 1$. In the next section, we improve these numerical results and make observations that will guide us in the asymptotic analysis near $\sigma = 1$. In particular, we identify regions of validity of different approximations and corresponding turning points.

3.2. **Numerical methods.** The blow-up profile is computed for a sequence of values of σ approaching one by continuation. We use a second-order finite difference scheme, together with a Newton solver to solve the system for a given value of σ. Each successful computation is used as a starting guess for the next smaller value of σ in the sequence. We also make use of Richardson extrapolation to improve upon computed quantities, such as the parameters a and b. We computed the solution over a range of σ from $\sigma = 2$ down to 1.044, below which our solver struggled. We report quantities computed from this interval, $\sigma \in [1.044, 2]$. Details on the numerical methods can be found in Appendix B.

3.3. **Numerical Observations.** Figure 1 shows the amplitude $|Q|$ near the origin for several values of σ close to 1, computed with the above method. As mentioned before, we see that $|Q|$ is highly asymmetric, decaying much f

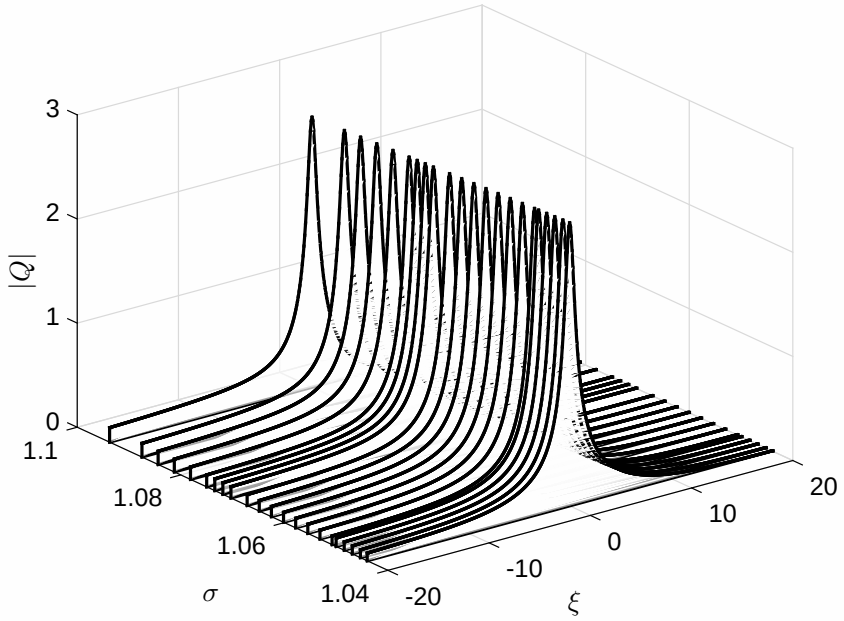

FIGURE 1. Amplitude $|Q|$ of the blowup profile for various values of σ close to 1.

As σ decreases, the parameter a decreases rapidly to zero and the profile Q tends to a soliton solution of the DNLS. The parameter b increases to a limiting value $b_0 \equiv \lim_{\sigma \to 1} b$. Recall that soliton solutions (2.3) and (2.4) to (2.2) are defined for $|b| < 2$ and $b = 2$ respectively. When $\sigma = 1$ and $|b| < 2$, the Hamiltonian of (2.1) (with $R = B_1$) is $H(B_1) = -b\sqrt{4 - b^2}$ and its momentum is $P(B_1) = -2\sqrt{4 - b^2}$, while when $b = 2$ (and $R = L_1$) both the energy and momentum vanish. By construction, the profile Q has a vanishing Hamiltonian and momentum. We thus make the Ansatz

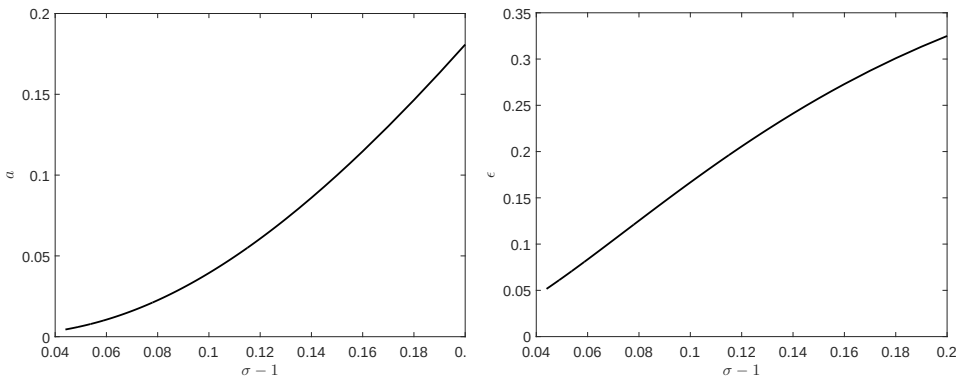

(a) a vs. σ (b) ϵ vs. σ

FIGURE 2. Numerically computed parameters a and $\epsilon = 2-b$ for a range of $\sigma \in [1.044, 1.2]$.

$\epsilon \equiv 2 - b \to 0$ while $\frac{\epsilon}{a} \gg 1$. We will show that this assumption leads to a consistent asymptotic analysis of all the parameters. The behaviour of a and ϵ for a range of values of σ is illustrated in Figure 2.

Turning to the amplitude and phase equations of Q, (2.9a) and (2.9b), we see in Figure 3 that $\psi \equiv (\arg P)_\xi$ is very small in a large region containing the origin and the modified profile P is essentially real. Rewriting (2.9a) in terms of ϵ gives

$$\begin{aligned} &A_{\xi\xi} + \left(\tfrac{1}{4}(a\xi+\epsilon)^2 - (a\xi+\epsilon) - \psi^2\right) A \\ &\qquad + \left(-1 + \tfrac{1}{2}(a\xi+\epsilon) - \tfrac{\sigma}{\sigma+1}\psi\right) A^{2\sigma+1} + \tfrac{2\sigma+1}{(2\sigma+2)^2} A^{4\sigma+1} = 0. \end{aligned} \tag{3.1}$$

If ψ is very small, the linear term in this equation reduces to

$$\left(\tfrac{1}{4}(a\xi+\epsilon)^2 - (a\xi+\epsilon)\right) A \tag{3.2}$$

which is negative if $\xi \in \left(-\frac{\epsilon}{a}, \frac{4-\epsilon}{a}\right)$. We thus define the turning points

$$\xi_- \equiv -\frac{\epsilon}{a}, \quad \xi_+ \equiv \frac{4-\epsilon}{a}. \tag{3.3}$$

Figure 3 shows how the behaviour of ψ changes near these points for several values of σ. For large $|\xi|$, the term (3.2) is positive, it must be compensated by ψ^2 to avoid oscillations of the amplitude. As $|\xi| \to \infty$, $\psi \approx \frac{a\xi}{2}$ and we confirm in Figure 3 that ψ achieves this behaviour when $|\xi|$ is much larger than the turning points.

We now consider the amplitude equation (3.1). For $0 \le \xi \ll \frac{\epsilon}{a}$, $a\xi + \epsilon \approx \epsilon$ and (3.1) essentially reduces to (2.2) satisfied by the bright soliton (2.3) with parameter $b = 2 - \epsilon$. On the negative side, for $\xi \le 0$, the terms $a\xi$ and ϵ work against each other and we find that the lump soliton (2.4) better approximates the solution. However, when ξ approaches $\xi_- = -\frac{\epsilon}{a}$, the phase becomes important and the amplitude deviates from (2.4) as shown

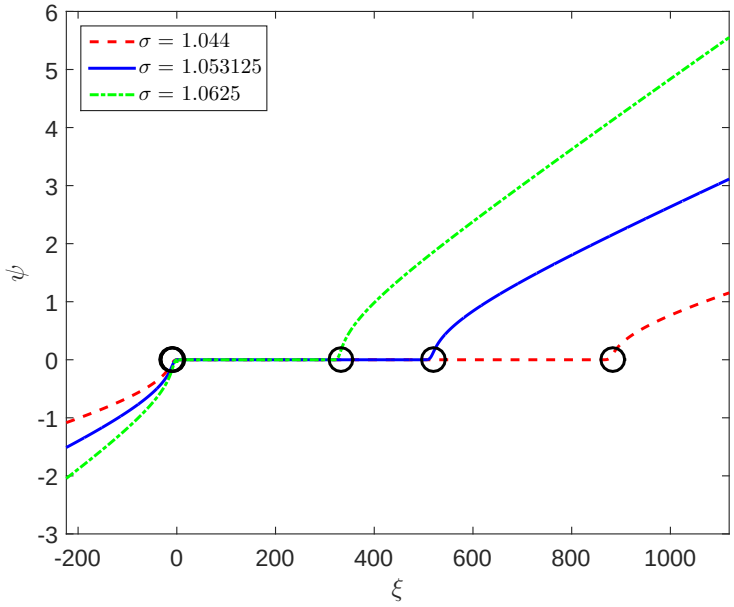

FIGURE 3. Phase derivative ψ at several values of σ. Note the change in behaviour near the turning points $\xi_- = -\frac{\epsilon}{a}$ and $\xi_+ = \frac{4}{a}$.

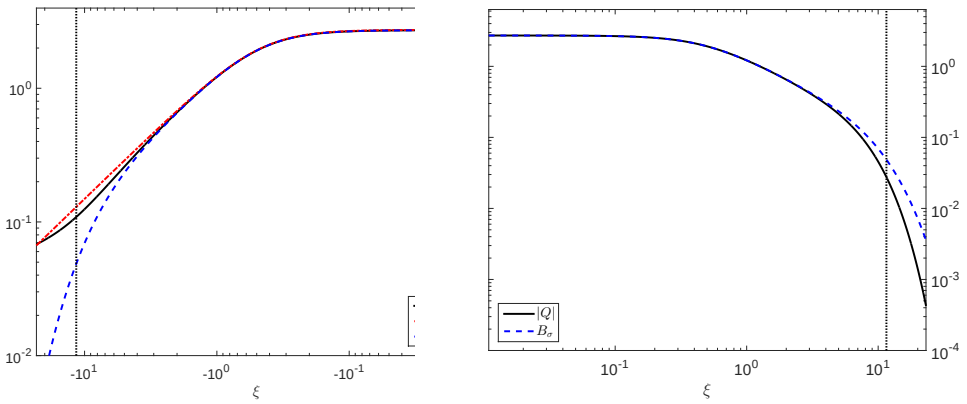

(a) (b)

FIGURE 4. $|Q|$ calculated at $\sigma = 1.044$ and compared to both the lump and bright solitons for $-\frac{\epsilon}{a} \leq \xi \leq 0$ (left) and the bright soliton for $0 \leq \xi \leq \frac{\epsilon}{a}$ (right). The vertical lines correspond to $|\xi| = \frac{\epsilon}{a}$

.

in Figure 4 (a). This deviation is a source of difficulty in the asymptotic

analysis. Figure 4 (b) displays $|Q|$ for $\xi > 0$ compared to the bright soliton (2.3).

Remark 3.1. *For $\xi \ll \epsilon^{-1/2}$, the bright and lump solitons nearly coincide.*

We are now in a position to better interpret the asymmetry of the profile amplitude. The turning point $\xi_+ \approx \frac{4}{a}$ grows very rapidly. When $1 \ll \xi < \xi_+$, the nonlinear terms in (3.1) are negligible and the negative linear term (3.2) forces the amplitude to decay very rapidly. Figure 5 shows the amplitude for several values of σ close to 1 and we clearly see this fast decay up to the turning point ξ_+. In this region the WKB method provides a good approximate solution. Meanwhile, on the negative side, $|\xi_-| = \frac{\epsilon}{a}$ grows moderately and the linear term is very small for $\xi \in (\xi_-, 0)$. We observe only a moderate decay of the amplitude for negative values of ξ. When $\xi < \xi_-$ away from the turning point, the WKB method provides a good approximation to the solution. Finally, when $|\xi|$ is large and far away from the turning points, the amplitude is well approximated by the leading order asymptotics $|Q| \approx A_\pm |\xi|^{-\frac{1}{2\sigma}}$.

In the next section, we derive a formal asymptotic analysis motivated by these observations and describe the leading order behaviour of the parameters a and ϵ as $\sigma \to 1$.

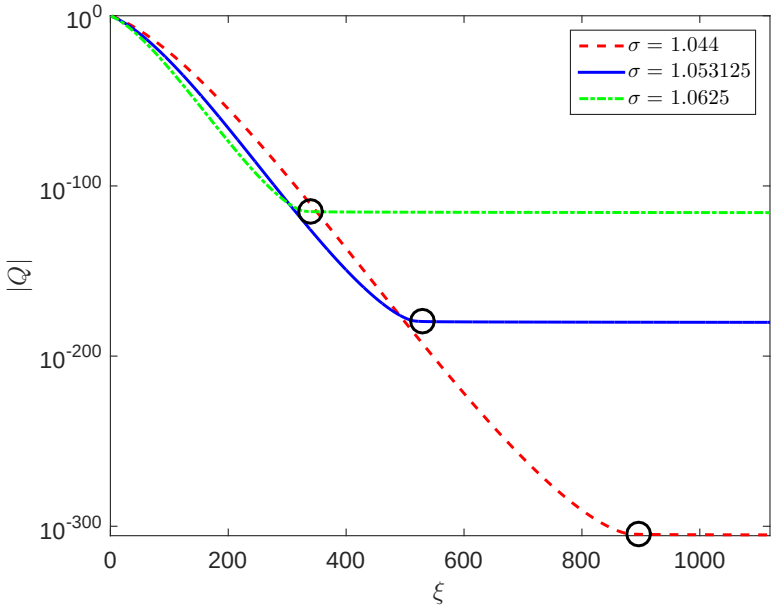

FIGURE 5. $|Q|$ computed at several values of σ. Note the rapid decay up to the turning point $\xi_+ = \frac{4}{a}$ marked with ◯.

.

4. Asymptotic analysis

The numerics indicate that, as $\sigma \to 1$, the parameters $a(\sigma)$, $b(\sigma)$ tend to 0 and 2 respectively, while the profile Q tends to the lump soliton (2.4). In this section, we investigate the deformation of Q and the parameters $a(\sigma)$, $b(\sigma)$ using asymptotic methods and analysis of the numerical data. In the course of the calculation, three additional parameters come into play, the coefficients A_+, A_- appearing in the large $|\xi|$ behaviour of Q (see equation(2.6)) and the derivative of the phase at the origin $\psi(0)$.

Section 4.1 concentrates on the region $\xi > 0$. We connect the bright soliton (2.3) which approximates P (defined in (2.7)) close to the origin to the asymptotic behaviour at large ξ (2.6) using WKB method. We obtain two relations between the above parameters, given in equations (4.1) and (4.24).

In Section 4.2 we examine the region $\xi < 0$. Close to the origin, the lump soliton (2.4) approximation is valid, however nonlinear effects become important near the turning point ξ_-. A precise analytic form of the profile in the (relatively small) region containing the turning point remains an open problem, nevertheless we are able to find a relation between the parameters (Eq (4.26)). Lacking a precise description of the profile in the intermediate region, we carefully analyze our numerical data and find that the turning point behaves like a power law in $(\sigma - 1)$: $a/\epsilon \sim (\sigma - 1)^\alpha$ with $\alpha \approx 1.2$. (Section 4.2.2.)

4.1. Asymptotic analysis of the profile for $\xi > 0$.

Proposition 4.1. *As $\sigma \to 1$, the behaviour of the coefficient A^+ defined in* (2.6) *is given by*

$$A_+ \approx 4\epsilon^{3/4} a^{-1/2} \exp\left\{ -\frac{\pi}{a} + \frac{2}{3}\frac{\epsilon^{3/2}}{a} \right\}. \tag{4.1}$$

Proof. We use the approach presented in Chapter 8 of [20] to connect the behaviour of Q as $\xi \to +\infty$ to the bright soliton approximation valid for $\xi \ll \frac{\epsilon}{a}$. First, we introduce the function S, which relates to Q by

$$S = Q \exp\left\{ i \left(\frac{a\xi^2}{4} - \frac{b\xi}{2} \right) \right\}. \tag{4.2}$$

S satisifies

$$S_{\xi\xi} - \left(1 - \tfrac{1}{4}(a\xi - b)^2\right) S - ia\tfrac{\sigma-1}{2\sigma} S + \tfrac{1}{2}(a\xi - b)|S|^{2\sigma} S + i|S|^{2\sigma} S_\xi = 0, \tag{4.3}$$

and as $\xi \to +\infty$,

$$S_{\text{Asymp}} = A_+ \xi^{\frac{-1}{2\sigma}} \exp\left\{ i \left(\frac{a\xi^2}{4} - \frac{b\xi}{2} - \frac{1}{a} \ln \xi \right) \right\}. \tag{4.4}$$

For sufficiently large $\xi \gg 1$, the nonlinear terms in (4.3) are negligible and we may write

$$S_{\xi\xi} = \left(1 - \tfrac{1}{4}(a\xi - b)^2\right) S. \tag{4.5}$$

Setting $x = \frac{1}{2}(a\xi - b)$, (4.5) becomes

$$\tfrac{a^2}{4} S_{xx} = (1 - x^2)S, \tag{4.6}$$

and the solution can be approximateed by the WKB method. For $x > 1$,

$$S^R_{\mathrm{WKB}} = \frac{1}{(x^2-1)^{\frac{1}{4}}} \left(C^R e^{i\left(\frac{\pi}{4} + \int_1^x \sqrt{s^2-1}ds\right)} + D^R e^{i\left(\frac{\pi}{4} - \int_1^x \sqrt{s^2-1}ds\right)} \right). \tag{4.7}$$

When $x \gg 1$,

$$\frac{2}{a}\int_1^x \sqrt{s^2-1}ds \approx \frac{1}{a}(x^2 - \ln x) \approx \frac{a\xi^2}{4} - \frac{b\xi}{2} - \frac{1}{a}\ln \xi, \tag{4.8}$$

implying that $D^R = 0$. Matching the amplitudes of (4.7) and (4.4), we find

$$C^R = \sqrt{\frac{a}{2}} A_+. \tag{4.9}$$

The right hand side of (4.6) vanishes at the turning point $x = 1$. The WKB approximation (4.7) is valid for $x - 1 \gg a^{\frac{2}{3}}$. If, in addition, $x - 1 \ll 1$, (4.7) can be simplified to

$$S^R_{\mathrm{WKB}} \approx \frac{C^R}{(2(1-x))^{\frac{1}{4}}} e^{i\left(\frac{\pi}{4} + \frac{4\sqrt{2}}{3a}(x-1)^{\frac{3}{2}}\right)}. \tag{4.10}$$

On the other hand, when $|x - 1| \ll 1$, we replace (4.6) by

$$\tfrac{a^2}{4} S_{xx} = 2(1 - x)S. \tag{4.11}$$

In the variable $t = 2a^{-\frac{2}{3}}(1 - x)$, (4.11) is the Airy equation

$$S_{tt} = tS \tag{4.12}$$

whose solution is $S_{\mathrm{Airy}} = a_1\,\mathrm{Ai}(t) + a_2\,\mathrm{Bi}(t)$. In terms of the variable t, the region $a^{\frac{2}{3}} \ll x - 1 \ll 1$ corresponds to $(-t) \gg 1$. Using the asymptotics of Ai and Bi as $t \to -\infty$,we obtain

$$S_{\mathrm{Airy}} \approx \frac{1}{\sqrt{\pi}(-t)^{\frac{1}{4}}} \left(a_1 \sin\left(\frac{\pi}{4} + \frac{2}{3}(-t)^{\frac{3}{2}}\right) + a_2 \cos\left(\frac{\pi}{4} + \frac{2}{3}(-t)^{\frac{3}{2}}\right)\right). \tag{4.13}$$

Matching the phases of (4.10) and (4.13) requires $a_1 = ia_2$, and matching the amplitudes gives

$$a_2 = a^{-\frac{1}{6}}\sqrt{\pi} C^R. \tag{4.14}$$

For $x < 1$, the region $1 \gg 1 - x \gg a^{\frac{2}{3}}$ corresponds to $t \gg 1$. Using the asymptotics of Ai and Bi as $t \to +\infty$, we obtain

$$S_{\text{Airy}} \approx \frac{1}{\sqrt{\pi} t^{\frac{1}{4}}} \left(\frac{a_1}{2} e^{\frac{-2}{3} t^{\frac{3}{2}}} + a_2 e^{\frac{2}{3} t^{\frac{3}{2}}} \right) \approx \frac{a_2}{\sqrt{\pi} t^{\frac{1}{4}}} e^{\frac{2}{3} t^{\frac{3}{2}}} \tag{4.15}$$

since the term with a negative exponent is negligible. On the other hand, solving (4.6) for $x < 1$ by WKB gives

$$S^L_{\text{WKB}} = \frac{1}{(1-x^2)^{\frac{1}{4}}} \left(C^L_1 e^{\frac{2}{a} \int_1^x \sqrt{1-s^2} ds} + C^L_2 e^{-\frac{2}{a} \int_1^x \sqrt{1-s^2} ds} \right). \tag{4.16}$$

Noting that for $(1 - x) \ll 1$

$$\frac{2}{a} \int_1^x \sqrt{1-s^2} ds \approx -\frac{4\sqrt{2}}{3a} (1-x)^{\frac{3}{2}}, \tag{4.17}$$

we have that for $1 \gg 1 - x \gg a^{\frac{2}{3}}$ (4.16) simplifies to

$$S^L_{\text{WKB}} \approx \frac{1}{(2(1-x))^{\frac{1}{4}}} \left(C^L_1 e^{-\frac{4\sqrt{2}}{3a} (1-x)^{\frac{3}{2}}} + C^L_2 e^{\frac{4\sqrt{2}}{3a} (1-x)^{\frac{3}{2}}} \right). \tag{4.18}$$

Finally, matching (4.18) to (4.15) and solving for $C^L \equiv C^L_2$ gives

$$a_2 = a^{-\frac{1}{6}} \sqrt{\pi} C^L, \tag{4.19}$$

where we have again ignored the term with a negative exponent. The approximation (4.16) for S is real valued and we connect it to the bright soliton approximation valid for $\xi \ll \frac{\epsilon}{a}$ as described in Section 3.3.

We assume here that $\epsilon \gg a^{\frac{2}{3}}$. This Ansatz will be checked a posteriori. The WKB approximation thus remains valid in some region included in $\xi < \frac{\epsilon}{a}$. Indeed, we work within the region $a^{-\frac{1}{3}} \ll \xi \ll \frac{\epsilon}{a}$, equivalently $a^{\frac{2}{3}} \ll x + 1 \ll \epsilon$. This condition also ensures that $\epsilon^{-\frac{1}{2}} \ll a^{-\frac{1}{3}}$ and the bright soliton can be approximated as

$$B_\sigma(\xi) \approx 2\sqrt{2\epsilon} e^{-\sqrt{\epsilon}\xi}. \tag{4.20}$$

In this region $1 - x^2 \approx 2(1 + x) = a\xi + \epsilon$, so we approximate

$$\int_1^x \sqrt{1-s^2} ds \approx -\frac{\pi}{2} + \frac{2\sqrt{2}}{3} (1+x)^{\frac{3}{2}} \approx -\frac{\pi}{2} + \frac{1}{3} \epsilon^{\frac{3}{2}} + \frac{1}{2} \sqrt{\epsilon} a \xi \tag{4.21}$$

and the WKB approximation (4.16) can be written as

$$S^L_{WKB} \approx C^L \epsilon^{-\frac{1}{4}} \exp\left\{ \frac{\pi}{a} - \frac{2}{3} \frac{\epsilon^{\frac{3}{2}}}{a} \right\} e^{-\sqrt{\epsilon}\xi}. \tag{4.22}$$

Matching (4.20) and (4.22) gives

$$C^L = 2\sqrt{2} \epsilon^{\frac{3}{4}} \exp\left\{ -\frac{\pi}{a} + \frac{2}{3} \frac{\epsilon^{\frac{3}{2}}}{a} \right\}. \tag{4.23}$$

Finally, combining relations (4.9), (4.14), (4.19) and (4.23), we obtain relation (4.1) between A_+, a, and ϵ.

□

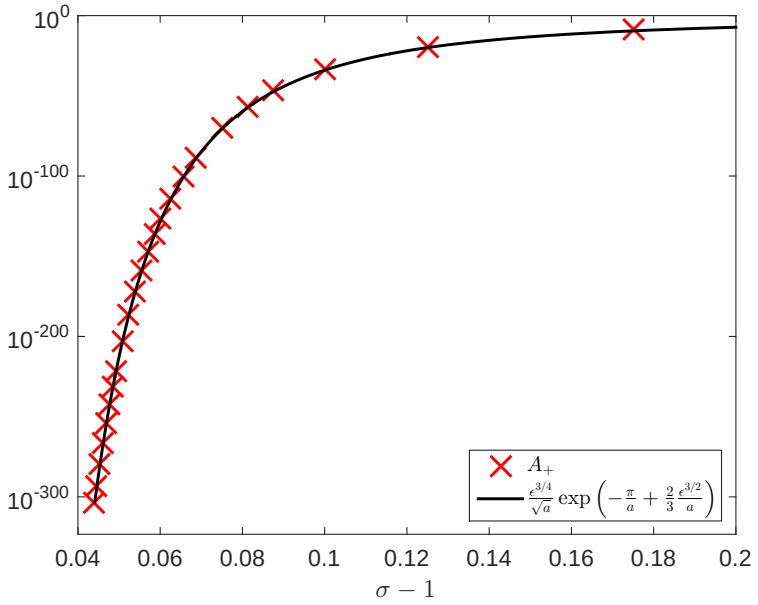

FIGURE 6. Numerical verification of (4.1) relating the coefficient A_+ to a and ϵ.

In Figure 6 we verify the relation (4.1) against the value of A_+ extracted from the numerical integration of the boundary value problem and find an excellent agreement for a large range of values σ from $\sigma = 1.2$ up to the limit of our computation at $\sigma = 1.044$.

Proposition 4.2. *To leading order in σ as $\sigma \to 1$, the derivative of the phase at the origin, $\psi(0)$, is given by*

$$\psi(0) \approx -\tfrac{\pi a}{8}(\sigma - 1)\,. \tag{4.24}$$

Proof. We turn to the relation (2.10) between the phase derivative ψ and the amplitude A. Take $\xi_0 > \frac{4}{a}$ sufficiently large so that $|Q(\xi_0)| \approx A_+ \xi^{\frac{-1}{2\sigma}}$, $\psi(\xi_0) \approx \frac{a\xi_0}{2}$, and denote $k \equiv \int_0^{\xi_0} A^2$. For $\xi > \xi_0$ we approximate (2.10) by

$$\begin{aligned}\psi(\xi) &\approx \frac{\psi(0)A^2(0)}{A_+^2}\xi^{\frac{1}{\sigma}} + \frac{a(\sigma-1)k}{2\sigma A_+^2}\xi^{\frac{1}{\sigma}} + \frac{a(\sigma-1)}{2\sigma A_+^2}\xi^{\frac{1}{\sigma}}\int_{\xi_0}^{\xi} A_+^2 \eta^{\frac{-1}{\sigma}} d\eta \\ &= \left(\frac{1}{A_+^2}\left(\psi(0)A^2(0) + \frac{a(\sigma-1)k}{2\sigma}\right) - \frac{a}{2}\xi_0^{1-\frac{1}{\sigma}}\right) + \frac{a\xi}{2}.\end{aligned}$$

Since A_+ decays exponentially fast, we have

$$\psi(0) \approx -\frac{a(\sigma-1)k}{2\sigma A^2(0)}. \tag{4.25}$$

The main contribution to the integral k comes from the region where the amplitude is approximated by the soliton, therefore to leading order as $\sigma \to 1$ we have $k \approx \int_0^\infty B_\sigma^2 \approx 2\pi$ and $A^2(0) \approx L_1(0) = 8$. □

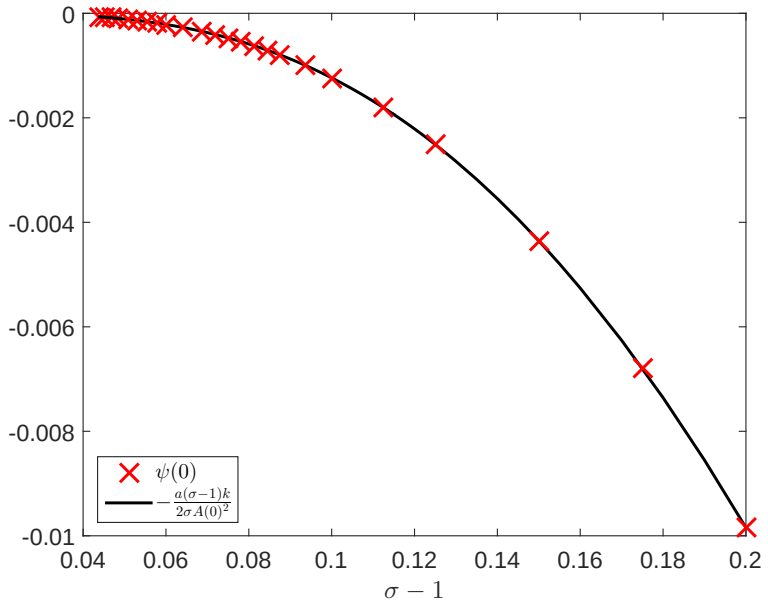

FIGURE 7. Numerical verification of relation (4.25) for $\psi(0)$ for a range of values of σ.

Figure 7 confirms the relation (4.25) against the numerical simulations, again finding excellent agreement. We check relation (4.25) rather than (4.24) because the values of σ at which we compute are insufficiently close to one for the constant k to have reach its limiting value.

4.2. **Asymptotic analysis of the profile for $\xi < 0$.**

4.2.1. *Asymptotics of the parameter A_-.*

Proposition 4.3. *To leading order in σ as $\sigma \to 1$, the coefficient A_- defined in (2.6) is given by*

$$A_- \approx \sqrt{4\pi\,(\sigma-1)}. \tag{4.26}$$

Proof. For sufficiently large $|\xi|$, $\xi < 0$, the function S satisfies (4.5) or, equivalently, defining $y = -\frac{1}{2}(a\xi - b)$,

$$\tfrac{a^2}{4} S_{yy} = (1-y^2)S. \tag{4.27}$$

Using WKB, we have for $y-1 \gg a^{\frac{2}{3}}$ (equivalently $|\xi - \frac{\epsilon}{a}| \gg a^{\frac{-1}{3}}$)

$$\arg(S) \approx \frac{\pi}{4} + \frac{2}{a}\int_1^y \sqrt{s^2-1}ds$$

from which it follows

$$\psi \approx -\sqrt{y^2-1}, \text{ and } A \approx \frac{\sqrt{\frac{a}{2}}A_-}{(y^2-1)^{\frac{1}{4}}}. \tag{4.28}$$

We improve the approximation of the amplitude by using (2.11), giving us

$$A \approx \frac{C_-}{(y^2-1)^{\frac{1}{4}}}\left(y+\sqrt{y^2-1}\right)^{\frac{\sigma-1}{2\sigma}}. \tag{4.29}$$

When $\xi \to -\infty$, $y \to +\infty$ and (4.29) becomes $A \approx \sqrt{2}C_- a^{-\frac{1}{2\sigma}}(-\xi)^{-\frac{1}{2\sigma}}$. Using Proposition 2.3, we have $A \approx A_-(-\xi)^{-\frac{1}{2\sigma}}$ when $\xi \to -\infty$. Thus the constants C_- and A_- are related by

$$C_- = \frac{a^{\frac{1}{2\sigma}}}{\sqrt{2}}A_-.$$

Returning to equation (2.10) for large negative $|\xi| \gg \frac{1}{a}$ and approximating A by its asymptotic behaviour we write

$$\begin{aligned}\psi(\xi) \approx & \frac{\psi(0)A^2(0)}{2\sigma A_-^2}|\xi|^{\frac{1}{\sigma}} + \frac{a(\sigma-1)}{2\sigma A_-^2}\left(\int_0^{-\frac{\epsilon}{a}-a^{-1/3}} A^2\right)|\xi|^{\frac{1}{\sigma}} \\ & - \left(1-\frac{1}{\sigma}\right)\frac{C_-^2}{A_-^2}|\xi|^{\frac{1}{\sigma}}\int_{1+a^{2/3}}^{\infty}\frac{\left(y'+\sqrt{y'^2-1}\right)}{\sqrt{y'^2-1}}dy'.\end{aligned} \tag{4.30}$$

We do not have a precise behaviour of the profile in the relatively small region between $-\frac{\epsilon}{a}$ and $-\frac{\epsilon}{a}-a^{-\frac{1}{3}}$, but we have numerically verified that the contribution of this small region to the above integrals is negligible compared to the contribution of the interval $(0,-\frac{\epsilon}{a})$. Denoting $l = \int_{-\frac{\epsilon}{a}}^0 A^2$ and using the expression (4.25) for $\psi(0)$, we write

$$\begin{aligned}\psi(\xi) &\approx -\frac{a(\sigma-1)(k+l)}{2\sigma A_-^2}|\xi|^{\frac{1}{\sigma}} - \left(1-\tfrac{1}{\sigma}\right)\frac{C^2}{A_-^2}\int_1^y \frac{\left(y'+\sqrt{y'^2-1}\right)}{\sqrt{y'^2-1}}dy' \\ &= \frac{1}{2}\left(a^{\frac{1}{\sigma}} - \frac{a(k+l)}{A_-^2}\left(1-\tfrac{1}{\sigma}\right)\right)|\xi|^{\frac{1}{\sigma}} + \frac{a\xi}{2}.\end{aligned} \tag{4.31}$$

Since $\psi(\xi) \sim \frac{a\xi}{2}$ as $\xi \to -\infty$, the coefficient of $|\xi|^{\frac{1}{\sigma}}$ vanishes and

$$A_-^2 = a^{1-\frac{1}{\sigma}}(k+l)\left(1-\tfrac{1}{\sigma}\right). \tag{4.32}$$

In the limit $\sigma \to 1$, $k \to 2\pi$ (see Proposition 4.2) while the main contribution to the integral $l = \int_{\epsilon/a}^0 A^2$ comes from the region $\left(-\frac{1}{2\sqrt{\epsilon}}, 0\right)$ where the DNLS soliton (2.3) approximates A (see Figure 8). Therefore

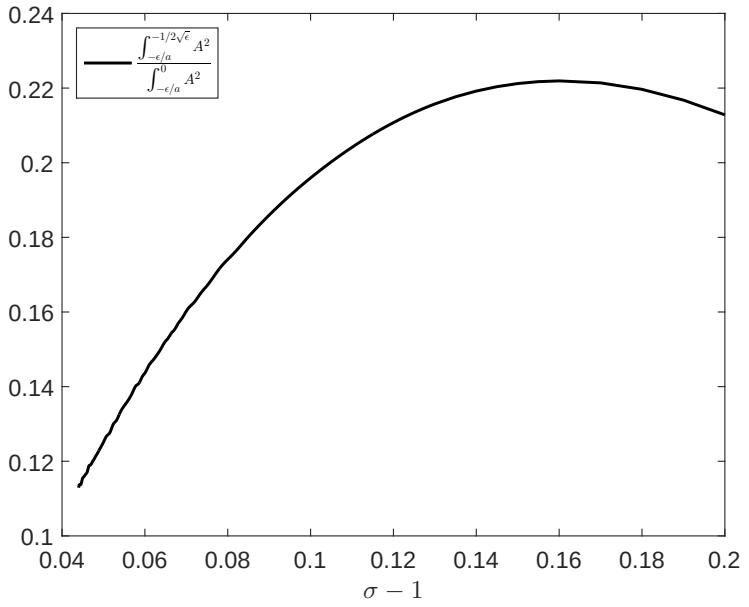

FIGURE 8. An estimate of the relative contribution of the region $\xi \in [-\epsilon/a, -1/2\sqrt{\epsilon}]$ (where the precise behaviour of the profile remains unknown) to the integral $l = \int_{-\epsilon/a}^{0} A^2$ appearing in (4.32)

$l \approx \int_{-\infty}^{0} L_1^2 = 2\pi$ and the relation (4.26) follows. In Figure 9, we observe an excellent agreement of the numerical simulation with the formula (4.32). Similar to our result for $\psi(0)$, we check (4.32) rather than (4.26) since for the values of σ we computed, the integrals k and l have not reached their limiting values.

□

4.2.2. *Variation of turning point ξ_- in terms of σ.* In the last section, we obtained the function Q for negative values of ξ that satisfy conditions of validity for the WKB method, namely $\xi < -\frac{\epsilon}{a}$ and $|\xi + \frac{\epsilon}{a}| > a^{-1/3}$. We also know that for $\xi < 0$ with $|\xi| \ll \frac{\epsilon}{a}$, the amplitude is well approximated by the DNLS soliton while the phase derivative ψ remains small. In order to match these behaviours we need to approximate Q in the intermediate region near $\xi \sim -\frac{\epsilon}{a}$. Unlike nearby the positive turning point $\xi_+ = \frac{4}{a}$, the problem here is fully nonlinear. The equation satisfied by P reduces to

$$P_{\xi\xi} \approx (a\xi + \epsilon)\, P + |P|^2 P \tag{4.33}$$

where both of the terms on the right hand side must be taken into account. This equation can be transformed to one resembling a type II Painlevé equation by setting $t = a^{-2/3}(a\xi + \epsilon)$ and $u = a^{-1/3}2^{-1/2}P$:

$$u_{tt} = tu + 2|u|^2 u.$$

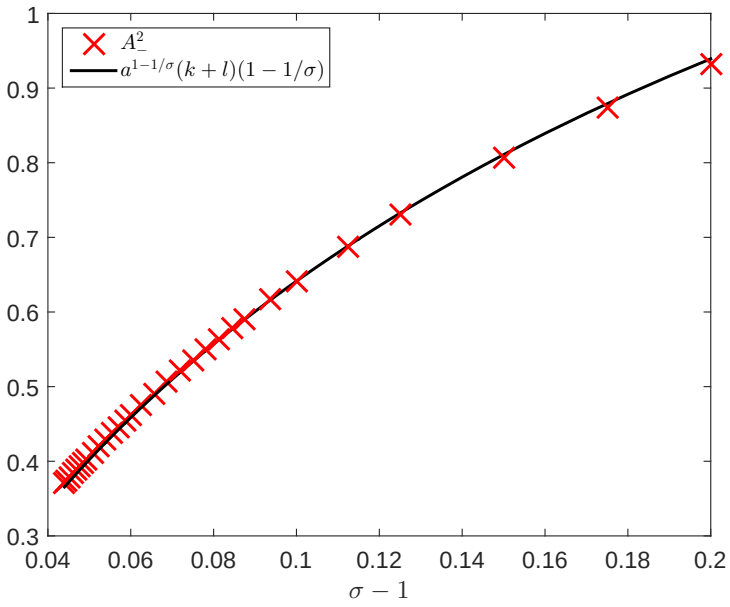

FIGURE 9. Numerical verification of (4.32) for A_- describing the asymptotic behaviour of Q as $\xi \to -\infty$.

The nonlinearity however is of the form $|u|^2u$ rather than the Painlevé u^3 and known results about approximate solutions to Painlevé do not apply.

Instead, we turn to our numerical data and examine the behaviour of the turning point as a function of σ. We will show in Section 5 that the parameter ϵ behaves as a power law in $(\sigma - 1)$ in the limit $\sigma \to 1$ and therefore make the Ansatz for ξ_-:

$$\frac{a}{\epsilon} \approx C\,(\sigma - 1)^{\alpha}\,, \quad \sigma \to 1. \tag{4.34}$$

We use a standard least squares algorithm to compute C and α and find $C \approx 4$ while $\alpha \approx 1.2$. Figure 10 illustrates the goodness of the fit for $\sigma \in [1.044, 1.1]$ with C and α obtained from a Richardson extrapolation of the values of a and ϵ from simulations with $N = 2.56\times10^6$ and $N = 5.12\times10^6$ mesh points and $\sigma \in [1.044, 1.1]$. To check the validity of this Ansatz, we change the range of σ values considered for the least square computation by restricting σ to $[1.044, \sigma_{max}]$ and varying σ_{max}. We do this for data obtained from simulations performed at several different resolutions and report the values obtained in Table 1. In the worst case, we observe relative differences in the values of C and α at the order of 0.1%.

5. VANISHING MOMENTUM CONDITION

In this Section, we use the zero momentum condition (2.5b) to obtain an additional relation between ϵ and σ in the limit $\sigma \to 1$. Combined with

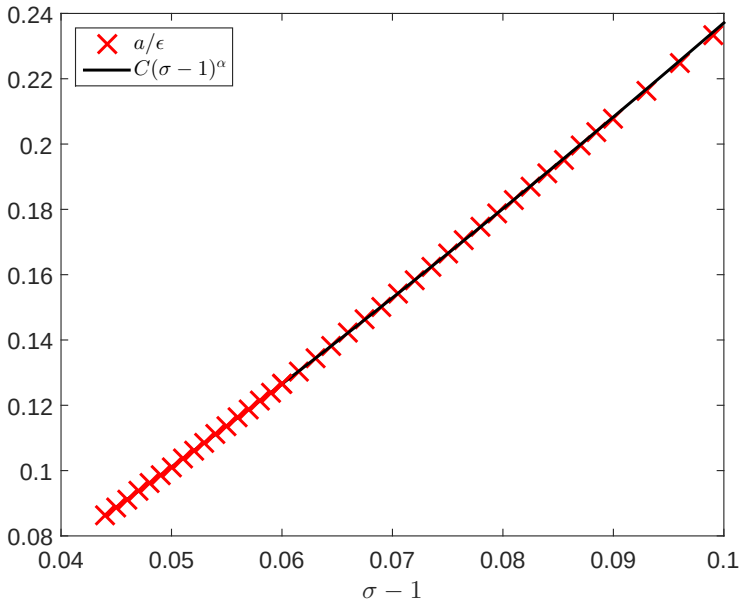

FIGURE 10. A numerical test of model (4.34) over a range of σ values. The values of C and α were computed using a least square analysis Within this range of σ, we find $C \approx 4.03$ and $\alpha \approx 1.23$.

TABLE 1. Computed values of parameters α, C in (4.34). Left: using simulations with $N = 5.12 \times 10^6$ and $N = 2.56 \times 10^6$ mesh points. Right: using simulations with $N = 1.28 \times 10^6$ and $N = 2.56 \times 10^6$ mesh points.

σ_{max}	α	C
1.100	1.2255	3.9754
1.095	1.2260	3.9809
1.090	1.2265	3.9873
1.085	1.2273	3.9959
1.080	1.2281	4.0049
1.075	1.2289	4.0149
1.070	1.2298	4.0253

σ_{max}	α	C
1.100	1.2253	3.9737
1.095	1.2258	3.9791
1.090	1.2263	3.9853
1.085	1.2270	3.9933
1.080	1.2279	4.0028
1.075	1.2286	4.0112
1.070	1.2294	4.0201

(4.34), it gives the main conclusion of this study as stated in equations (1.15) and (1.17).

Proposition 5.1. *As $\sigma \to 1$, the parameter ϵ satisfies, at leading order,*

$$\sqrt{\epsilon} \sim C\pi\,(\sigma - 1) \tag{5.1}$$

for some constant $2 < C < \frac{24}{7}$.

Proof. In terms of phase and amplitude, $Q = Ae^{i\theta}$, the property $I(Q) = 0$ has the form

$$I(Q) \equiv \int_{-\infty}^{\infty} \mathcal{I}(Q) d\xi = \int_{-\infty}^{\infty} \theta_\xi A^2 d\xi = 0. \tag{5.2}$$

We separate the domain into three regions: *(i)* $-\infty < \xi \lessapprox \frac{-\epsilon}{a}$; *(ii)* $\xi > 0$; *(iii)* $\frac{-\epsilon}{a} \lessapprox \xi < 0$ and denote I_1, I_2 and I_3 the corresponding contributions to I. In each region, we approximate the phase and amplitude of Q using the analysis of the previous sections.

Region 1: When $-\infty < \xi \leq -\frac{\epsilon}{a}$, we change variables to $y = -\frac{1}{2}(a\xi - b)$ and write

$$I_1 = \int_{-\infty}^{-\frac{\epsilon}{a}} \theta_\xi A^2 d\xi = \frac{2}{a} \int_1^{\infty} \theta_\xi A^2 dy \tag{5.3}$$

For $y - 1 \gg a^{\frac{2}{3}}$, A and θ_ξ are well approximated by (4.28). Since $\theta_\xi \approx \psi - \frac{1}{2}(a\xi - b) = \psi + y$, we have

$$A \approx \frac{a^{\frac{1}{2\sigma}} A_-}{\sqrt{2}(y^2-1)^{\frac{1}{4}}} \left(y + \sqrt{y^2-1}\right)^{\frac{\sigma-1}{2\sigma}}; \quad \theta_\xi \approx y - \sqrt{y^2-1}. \tag{5.4}$$

The contribution of the region $1 \leq y - 1 \leq a^{\frac{2}{3}}$, equivalently $-\frac{\epsilon}{a} - a^{-\frac{1}{3}} \leq \xi \leq -\frac{\epsilon}{a}$ (where the WKB analysis leading to (5.4) is no longer valid) to I is negligible compared to that of the region $y > 1 + a^{\frac{2}{3}}$. In Figure 11 we compare the values of I_1 obtained from the numerical integration of the solution to the boundary value problem (BVP) to those obtained by inserting (5.4) into (5.3). We see a good agreement with a relative error of less than 1%. The leading order contribution to I_1 is therefore

$$\frac{2}{a} \int_{1+a^{\frac{2}{3}}}^{\infty} \frac{\frac{a}{2} A_-^2 \left(y - \sqrt{y^2-1}\right)}{\sqrt{y^2-1}} dy \approx A_-^2.$$

Using Propositon 4.3 we have

$$I_1 \approx 4\pi(\sigma - 1), \quad \sigma \to 1. \tag{5.5}$$

Remark. Our numerical integration of the BVP did not reach values of σ sufficiently close to 1 to allow a direct check of this relation.

Region 2: When $\xi > 0$, our simulations tell us that the amplitude A is well approximated by the bright soliton (2.3) as long as $\xi \ll \frac{\epsilon}{a}$ with its region of validity extending at least to $\xi = a^{\frac{-1}{3}}$ (see Figure 4). For $\xi > \xi_+$, we can approximate A using WKB, with an amplitude that is exponentially small as $a \to 0$ (see Proposition 4.1). Consequently, the contribution to I_2 of the entire region $\xi > a^{-1/3}$ is exponentially small; for $\xi \in (a^{-1/3}, \xi_+)$, it is small because

$$A(\xi) \leq B_\sigma(a^{\frac{-1}{3}}) \approx \sqrt{\epsilon} \exp\left(-\sqrt{\epsilon} a^{\frac{-1}{3}}\right),$$

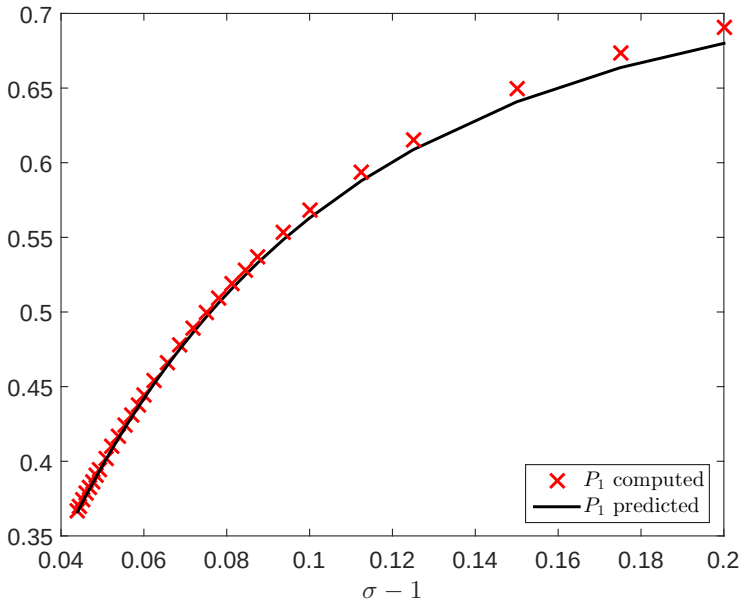

FIGURE 11. Comparison of the values of P_1 obtained from the numerical simulation with those obtained from (5.4).

while for $\xi > \xi_+$, it will be small exponentially small because A_+ is small (Proposition 4.1). In both regimes, we can make use of (4.34), relating a to ϵ and $\sigma - 1$. The consequence of this analysis is that the leading order contribution to I_2 is in $\xi < a^{-1/3}$, where the amplitude and phase derivative can be approximated by

$$A \approx B_\sigma = \left(\frac{(\sigma+1)(4-b^2)}{2\left(\cosh \sigma \sqrt{4-b^2}\xi - \frac{b}{2}\right)} \right)^{\frac{1}{2\sigma}}; \quad \theta_\xi \approx \frac{b}{2} - \frac{1}{2\sigma+2} B_\sigma^{2\sigma}. \tag{5.6}$$

We have omitted the $a\xi/2$ term from the phase derivative because it's contribution to the integral for $\xi < a^{-1/3}$ is $\mathrm{O}(a^{1/3}) \ll \sqrt{\epsilon}$. Under the assumption that $\sqrt{\epsilon} \propto \sigma - 1$, which will be our conclusion, $\mathrm{O}(a^{1/3}) \ll \sigma - 1$, so the term will be small relative to the main contributions to the integral, which are $\mathrm{O}(\sqrt{\epsilon})$ and $(\sigma - 1)$. Thus, the contribution of this region to the momentum is approximated as

$$\begin{aligned} I_2 \approx \int_0^{a^{-1/3}} \mathcal{I} &\approx \int_0^{a^{-1/3}} \left(\frac{b}{2} - \frac{1}{2\sigma+2} B_\sigma^{2\sigma} \right) B_\sigma^{2\sigma} \\ &\approx \int_0^{\infty} \left(\frac{b}{2} - \frac{1}{2\sigma+2} B_\sigma^{2\sigma} \right) B_\sigma^{2\sigma} \end{aligned} \tag{5.7}$$

The final approximation is due to the integral over $(a^{-1/3}, \infty)$ of the approximate density being $\ll \sqrt{\epsilon}$. Thus we include it for the convenience of analytical integration.

Using these approximations, we expand I_2 as

$$I_2 \approx I_2(\sigma, \epsilon) \mid_{\sigma=1} + (\sigma - 1)\frac{\partial I_2}{\partial \sigma}(\sigma, \epsilon) \mid_{\sigma=1}$$

By direct integration,

$$I_2(\sigma, \epsilon) \mid_{\sigma=1} = \int_0^\infty \left(\frac{b}{2} - \frac{B_1^2}{4}\right) B_1^2 d\xi = -\sqrt{4 - b^2} \approx -2\sqrt{\epsilon}. \tag{5.8}$$

The second term in the expansion is given by

$$\left.\frac{\partial I_2}{\partial \sigma}\right|_{\sigma=1} \approx \int_0^\infty \frac{\partial}{\partial \sigma}\left[\left(\frac{b}{2} - \frac{B_\sigma^{2\sigma}}{2\sigma + 2}\right) B_\sigma^2\right]\Bigg|_{\sigma=1} d\xi. \tag{5.9}$$

To approximate this integral, we first claim that the main contribution comes from $\xi < \frac{1}{\sqrt{4-b^2}} \approx \frac{1}{2\sqrt{\epsilon}}$. To see this, we note that the bright soliton B_σ is a function of $u = \sigma\sqrt{4 - b^2}\xi \approx 2\sqrt{\epsilon}\xi$ and take great care when differentiating with respect to σ under the integral sign. To wit, we split the integral into 2 parts at $\xi_0 = \frac{1}{\sigma\sqrt{4-b^2}}$ and write

$$\begin{aligned}\left.\frac{\partial I_2}{\partial \sigma}\right|_{\sigma=1} = &\underbrace{\int_0^{\xi_0} \frac{\partial}{\partial \sigma}\left[\left(\frac{b}{2} - \frac{B_\sigma^{2\sigma}}{2\sigma + 2}\right) B_\sigma^2\right]\Bigg|_{\sigma=1} d\xi}_{\equiv I_{2,1}} \\ &+ \underbrace{\xi_0^{-1} \int_1^\infty \frac{\partial}{\partial \sigma}\left[\left(\frac{b}{2} - \frac{B_\sigma^{2\sigma}}{2\sigma + 2}\right) B_\sigma^2\right]\Bigg|_{\sigma=1} du}_{\equiv I_{2,2}}.\end{aligned} \tag{5.10}$$

We now observe that the second integral, $I_{2,2}$, tends to zero as $\sigma \to 1$ while the first tends to a finite value. Indeed, via direct computation, we obtain

$$\begin{aligned} I_{2,2} &\approx \frac{1}{2\sqrt{\epsilon}} \int_1^\infty \left(\frac{b}{2} - \frac{B_1^2}{4}\right)\left(\frac{1}{2}B_1^2 - 2B_1^2 \log B_1\right) du \\ &\approx \frac{1}{\sqrt{\epsilon}}\left(c_1 \epsilon \log \epsilon + c_2 \epsilon + O(\epsilon^2)\right) \\ &\approx c_1\sqrt{\epsilon}\log\epsilon + c_2\sqrt{\epsilon} \end{aligned} \tag{5.11}$$

where B_1 is the bright soliton with $\sigma = 1$ and $c_1 \approx -2.33$ and $c_2 \approx -0.66$ are constant values. Under the Ansatz that ϵ behaves as a power law in $(\sigma - 1)$, $I_{2,2}$ tends slowly to zero. For $I_{2,1}$, the bright soliton nearly coincides with

the lump and we have by direct computation

(5.12)
$$\begin{aligned} I_{2,1} &\approx \int_0^{1/2\sqrt{\epsilon}} \left\{ \frac{B_1^6 \xi \sinh\sqrt{4-b^2}\xi}{4\sqrt{4-b^2}} \right. \\ &\qquad \left. + \left(\frac{b}{2} - \frac{B_1^2}{4}\right)\left(-2B_1^2 \ln B_1 + \frac{B_1^2}{2} - \frac{B_1^4 \xi \sinh\sqrt{4-b^2}\xi}{\sqrt{4-b^2}}\right)\right\} d\xi. \\ &\approx \int_0^{\infty} \left\{ \frac{\xi^2 L_1^6}{4} + \left(1 - \frac{L_1^2}{4}\right)\left(-2L_1^2 \ln L_1 + \frac{L_1^2}{2} - \xi^2 L_1^4\right)\right\} d\xi \\ &= 2\pi, \end{aligned}$$

where we take the limit $\epsilon \to 0$ in the penultimate step. Using (5.8) and (5.12), we conclude that

$$I_2 \approx -2\sqrt{\epsilon} + 2\pi(\sigma - 1), \quad \sigma \to 1. \tag{5.13}$$

Region 3: Near the origin, for $\xi < 0$, the amplitude is well approximated by the bright soliton. However, as we approach ξ_-, the linear term $(a\xi + \epsilon)P$ in (2.8) becomes less relevant and the lump soliton becomes a better approximation . We thus subdivide the integral I_3 into the regions $-\frac{1}{2\sqrt{\epsilon}} < \xi < 0$ and $-\frac{\epsilon}{a} < \xi < -\frac{1}{2\sqrt{\epsilon}}$.

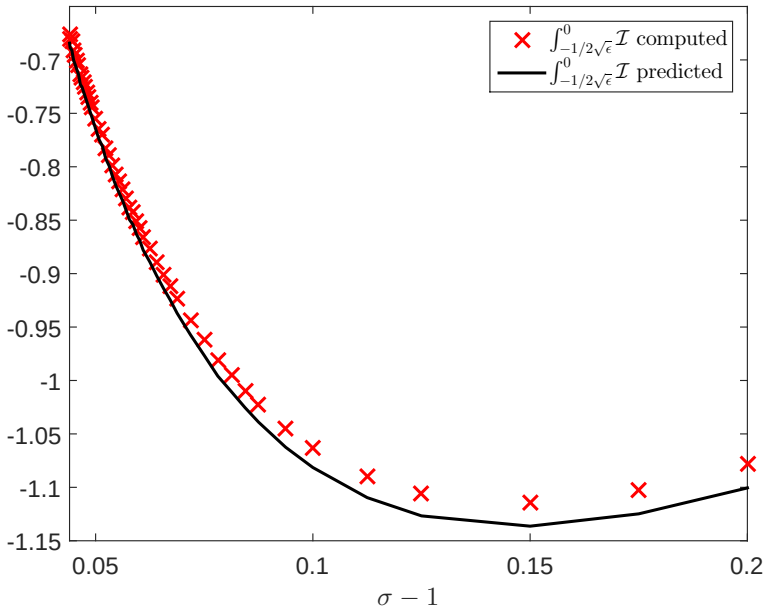

FIGURE 12. A comparison of the contribution to the momentum P of the region $[-\frac{1}{2\sqrt{\epsilon}}, 0]$ from the numerical solution to that predicted by the bright soliton approximation.

Figure 12 compares the contribution to the momentum, over the interval $-\frac{1}{2\sqrt{\epsilon}} < \epsilon < 0$, between the numerical solution and approximation (5.6), using the bright soliton. We find that they are in good agreement over a range of values of σ with a relative error of less than 2%. Therefore we approximate the contribution of this interval by calculating $\int_{-\frac{1}{2\sqrt{\epsilon}}}^{0} \mathcal{I}(B_\sigma)$ to leading order. When $-\frac{1}{2\sqrt{\epsilon}} < \xi < 0$, we expand the bright soliton near $\sigma = 1, \epsilon = 0$ as

$$B_\sigma(\xi) = L_1(\xi) + (\sigma - 1) f_1(\xi) + \epsilon f_2(\xi) \tag{5.14}$$

where L_1 is the lump soliton ($\sigma = 1$) and f_1, f_2 are given by

$$\begin{aligned} f_1(\xi) &= -\frac{1}{\sqrt{2}} \left(\frac{1}{4\xi^2 + 1} \right)^{3/2} \left[12\xi^2 + \left(8\xi^2 + 2 \right) \log \left(\frac{8}{4\xi^2 + 1} \right) - 1 \right], \\ f_2(\xi) &= -\frac{16\xi^4 + 3}{6\sqrt{2} \left(4\xi^2 + 1 \right)^{3/2}}. \end{aligned} \tag{5.15}$$

The contribution of this interval to I_3 becomes

$$\int_{-\frac{1}{2\sqrt{\epsilon}}}^{0} \mathcal{I}(B_\sigma) \approx \int_{-\frac{1}{2\sqrt{\epsilon}}}^{0} \mathcal{I}_0 + (\sigma - 1) \int_{-\frac{1}{2\sqrt{\epsilon}}}^{0} \mathcal{I}_1 + \epsilon \int_{-\frac{1}{2\sqrt{\epsilon}}}^{0} \mathcal{I}_2$$

where the integrands are computed at leading order using (5.14):

$$\begin{aligned} \mathcal{I}_0 &= \left(1 - \frac{L_1^2}{4} \right) L_1^2 \\ \mathcal{I}_1 &= 2 L_1 f_1 \left(1 - \frac{L_1^2}{4} \right) - \frac{1}{2} \left(L_1 f_1 + L_1^2 \ln L_1 - \frac{L_1^2}{4} \right) L_1^2 \\ \mathcal{I}_2 &= 2 f_2 L_1 \left(1 - \frac{L_1^2}{4} \right) - \frac{1}{2} \left(f_2 L_1 + 1 \right) L_1^2. \end{aligned}$$

Using Mathematica, we find:

$$\int_{-\frac{1}{2\sqrt{\epsilon}}}^{0} \mathcal{I}_0 \approx -4\sqrt{\epsilon}, \quad \int_{-\frac{1}{2\sqrt{\epsilon}}}^{0} \mathcal{I}_1 \approx 2\pi, \quad \int_{-\frac{1}{2\sqrt{\epsilon}}}^{0} \mathcal{I}_2 \approx -\frac{1}{3\sqrt{\epsilon}}. \tag{5.16}$$

To summarize, we have

$$\int_{-\frac{1}{2\sqrt{\epsilon}}}^{0} \mathcal{I}(B_\sigma) \approx -\frac{13}{3}\sqrt{\epsilon} + 2\pi(\sigma - 1).$$

For $-\frac{\epsilon}{a} < \xi < -\frac{1}{2\sqrt{\epsilon}}$, the bright soliton is not a valid approximation of the amplitude. Although we do not have a precise analytic expression of Q throughout this region, we observe, as illustrated in Figure 13, that

$$\int_{-\frac{\epsilon}{a}}^{-\frac{1}{2\sqrt{\epsilon}}} \mathcal{I}(L_\sigma) > \int_{-\frac{\epsilon}{a}}^{-\frac{1}{2\sqrt{\epsilon}}} \mathcal{I} > \int_{-\frac{\epsilon}{a}}^{-\frac{1}{2\sqrt{\epsilon}}} \mathcal{I}(B_\sigma).$$

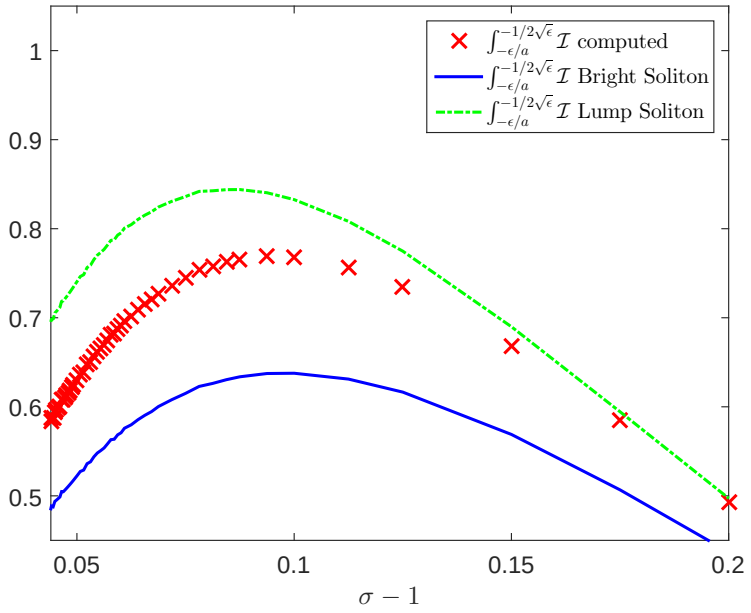

FIGURE 13. Comparison of the contribution to the momentum of the region $[-\frac{\epsilon}{a}, -\frac{1}{2\sqrt{\epsilon}}]$ obtained in the simulation with the same quantity using the bright soliton and using the lump soliton approximations.

When $\sigma \to 1$, $L_\sigma \approx L_1 + (\sigma - 1) f_1$ with f_1 as in (5.15) and

$$\int_{-\frac{\epsilon}{a}}^{-\frac{1}{2\sqrt{\epsilon}}} \mathcal{I}(L_\sigma) \approx 4\sqrt{\epsilon}.$$

On the other hand, $\int_{-\frac{\epsilon}{a}}^{-\frac{1}{2\sqrt{\epsilon}}} \mathcal{I}(B_\sigma)$ can be estimated by the same methods as in Region 2. Indeed, recognizing that the density $\mathcal{I}(B_\sigma)$ is even in ξ,

$$\int_{-\frac{\epsilon}{a}}^{0} \mathcal{I}(B_\sigma) = \int_{0}^{\frac{\epsilon}{a}} \mathcal{I}(B_\sigma) \approx \int_{0}^{\infty} \mathcal{I}(B_\sigma) \approx 2\pi(\sigma - 1) - 2\sqrt{\epsilon}.$$

Combining the bounds and estimates for the two pieces of Region 3,

$$\int_{-\frac{\epsilon}{a}}^{-\frac{1}{2\sqrt{\epsilon}}} \mathcal{I}(B_\sigma) \approx \frac{7\sqrt{\epsilon}}{3},$$

which gives us

$$I_2 \sim 2\pi(\sigma - 1) - \mu\sqrt{\epsilon} \tag{5.17}$$

where μ is some constant satisfying $\frac{1}{3} < \mu < 2$.

Combining the 3 regions, namely (5.5), and (5.13) and (5.17), we find that

$$I(Q) \sim 8\pi(\sigma - 1) - (\mu + 2)\sqrt{\epsilon}.$$

We now impose the vanishing momentum condition to get the main result of this section:

$$\sqrt{\epsilon} \sim \frac{8\pi}{\mu+2}(\sigma-1), \quad 1/3 < \mu < 2. \tag{5.18}$$

We are unable to numerically check the leading order behaviour of ϵ in Eq. (5.18) directly because we have not reached values of σ sufficiently close to 1 to ignore higher order corrective terms on the right hand side. Indeed, as exhibited in (5.11), the corrections may be of intermediate order, and they significantly affect the numerics. For this reason, we include a term of the form $f(\sigma) \sim (\sigma-1)^2 \log(\sigma-1)$ in the right hand side of (5.18) and make the Ansatz

$$\sqrt{\epsilon} = \left(C_0 + C_1 (\sigma-1)\log(\sigma-1)\right)(\sigma-1)^{\alpha}. \tag{5.19}$$

We then use a nonlinear least squares algorithm to calculate C_0, C_1 and α. We find that $C_0 \approx 8$, $C_1 \approx 15$ and $\alpha \approx 1$ (the latter being the result derived in (5.18) analytically). The value $C_0 \approx 8$ corresponds to $\mu \approx 1.1$ in (5.18), well within the predicted range. Figure 14 illustrates the goodness of the fit of (5.18) for $\sigma \in [1.035, 1.1]$ and values of C_0, C_1, and α obtained by a least square analysis of Richardson extrapolation of ϵ values from computations using $N = 2.56 \times 10^6$ and $N = 5.12 \times 10^6$ mesh points. To check the validity of the obtained values we proceed as for the model (4.34): we restrict the values of σ considered in the least square analysis to $\sigma \in [1.044, \sigma_{max}]$ and vary σ_{max}. We also use results from computations performed at different resolutions and report the values obtained in Table 2. In the worst case, we observe a relative difference between the obtained values on the order of 4%.

TABLE 2. A table of computed values for the parameters α, C_0 and C_1 in (5.19). Left: using simulations with $N = 5.12 \times 10^6$ and $N = 2.56 \times 10^6$ mesh points. Right: using simulations with $N = 1.28 \times 10^6$ and $N = 2.56 \times 10^6$ mesh points.

σ_{max}	α	C_0	C_1
1.100	1.045	8.037	15.226
1.095	1.045	8.020	15.177
1.090	1.044	8.004	15.128
1.085	1.043	7.984	15.070
1.080	1.043	7.963	15.006
1.075	1.042	7.942	14.940
1.070	1.041	7.915	14.859

σ_{max}	α	C_0	C_1
1.100	1.044	8.013	15.161
1.095	1.044	7.994	15.103
1.090	1.043	7.972	15.039
1.085	1.042	7.945	14.957
1.080	1.041	7.922	14.887
1.075	1.040	7.891	14.790
1.070	1.039	7.854	14.677

□

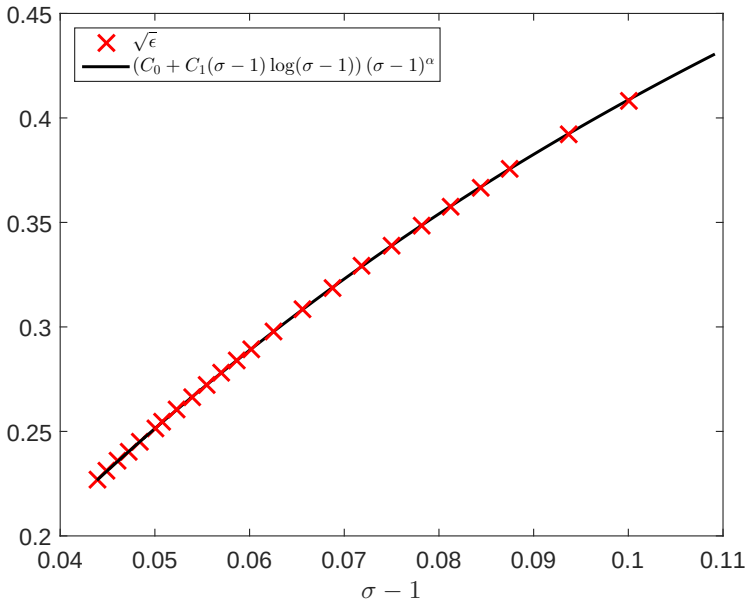

FIGURE 14. Numerical verification of model (5.19) using a least square computation to find the parameters C_0, C_1, and α. We find that $C_0 \approx 7.915$, $C_1 \approx 14.859$ and $\alpha \approx 1.041$.

Remark: It is possible to prove Proposition 5.1 by considering the condition $H(Q) = 0$ (see (2.5a) in place of $P(Q) = 0$. Using the same analysis and separation of the domain, we obtain $H_1 \sim 2\pi(\sigma - 1)$, $H_2 \sim 3\pi(\sigma - 1) - 2\sqrt{\epsilon}$ and $H_3 \sim 3\pi(\sigma - 1) - \mu\sqrt{\epsilon}$. We omit the details of this calculation as the Hamiltonian density is a more complicated object while the final result (5.1) is unchanged.

6. Discussion and further remarks

Combining Proposition 5.1 and the numerical fit (4.34) gives us the central result of this study: that in the limit $\sigma \to 1$, $a(\sigma)$ behaves as a power law with respect to the distance to criticality $(\sigma - 1)$ (that is $a \sim (\sigma - 1)^\alpha$ with $\alpha \approx 3.2$), while the amplitude of the blow-up profile tends to the lump soliton of DNLS. In the course of the analysis, we have made several assumptions on the relative behaviours of a and ϵ that we now check a posteriori. We have assumed that $a^{2/3} \ll \epsilon$, $\frac{a}{\epsilon} \ll \sigma - 1$ and $\epsilon \ll (\sigma - 1)$, all consistent with our final result.

In some cases, we did not check the asymptotic relations directly against our numerical simulation because although we reach values of σ as low as $\sigma = 1.044$, we cannot ignore some of the higher order corrections. For example, in Propositions 4.1, 4.2 and 4.3, we derived the form of the parameters A_+, $\psi(0)$ and A_- (through equations (4.1), (4.25) and (4.32)) that have more than leading order precision and we find excellent agreement with the

numerical simulations. In Section 4.2.2 however, we were restricted to a heuristic discussion in a neighborhood of the turning point $\xi_- = -\frac{\epsilon}{a}$. The behaviour of the profile here is a result of a delicate balance of linear and nonlinear terms in (4.33) and its precise analytic description remains an open problem. Finally, in Proposition 5.1, we estimated the integral constraint $P = \int \theta_\xi A^2 = 0$ using the approximations of the preceding sections. We use the DNLS solitons (2.4) and (2.3) to bound explicitly above and below the integral over the neighborhood of ξ_- where nonlinear effects are important. We obtain relation (5.1); however, the constant of proportionality is not known precisely.

Appendix A. Details of the Asymptotic Expansion

This Appendix contains the proof of Proposition 2.3 which is a slight extension of Proposition 4.1 in [12]. We decompose the blowup profile as $Q = XZ$, where X is a phase term chosen to remove linear terms in Z_ξ. Let

$$X(\xi) = \exp\left\{-i\left(\frac{a\xi^2}{4} - \frac{b\xi}{2} + \frac{1}{2}\int_0^\xi |Z(\xi')|^{2\sigma} d\xi'\right)\right\}, \tag{A.1}$$

Z satisfies

$$Z_{\xi\xi} + \left(\frac{1}{4}(a\xi - b)^2 + \frac{1}{2}(a\xi - b)|Z|^{2\sigma} + \frac{|Z|^{4\sigma}}{4} - 1 - i\frac{a(\sigma-1)}{2\sigma} - \frac{i}{2}\left(|Z|^{2\sigma}\right)_\xi\right) Z = 0. \tag{A.2}$$

Decomposing Z into phase and amplitude, $Z = Ae^{i\phi}$, gives

$$\frac{A_{\xi\xi}}{A} - \phi_\xi^2 - 1 + \frac{1}{4}(a\xi - b)^2 + \frac{1}{2}(a\xi - b)A^{2\sigma} + \frac{A^{4\sigma}}{4} = 0 \tag{A.3}$$

$$\phi_{\xi\xi} + 2\frac{A_\xi}{A}\phi_\xi - \frac{a(\sigma-1)}{2\sigma}A - \frac{1}{2}\left(A^{2\sigma}\right)_\xi = 0. \tag{A.4}$$

Let $\theta \equiv \phi_\xi$. Following [12], we now assume that, as $\xi \to \pm\infty$,

$$\theta(\xi) = \frac{a\xi - b}{2} - \frac{1}{a\xi} - \frac{b^2}{a^2\xi^2} + \frac{1}{2}A^{2\sigma} + \gamma(\xi), \quad \gamma(\xi) = \mathrm{O}(\xi^{-3}), \tag{A.5}$$

$$A(\xi) = A_\pm\,|\xi|^{-\frac{1}{2\sigma}}\left(1 + \frac{b}{2a\sigma\xi} + \nu(\xi)\right), \quad \nu(\xi) = \mathrm{O}(\xi^{-2}). \tag{A.6}$$

$\gamma(\xi)$ and $\nu(\xi)$ are corrections to the terms explicitly written. While we have made an assumption as to their order as $\xi \to \pm\infty$, they remain undetermined at this point. We will also assume that they are smooth, and their derivatives obey

$$\gamma^{(n)}(\xi) = \mathrm{O}(\xi^{-3-n}), \quad \nu^{(n)}(\xi) = \mathrm{O}(\xi^{-2-n}).$$

We substitute (A.5) and (A.6) into (A.3) and (A.4). We must show that the corrections, with the assumed orders, are consistent; there must be other terms in the equations which can balance them. Then, in principle, we could successively solve for the next correction. One subtlety is that in (A.5) and in the terms $A^{2\sigma}$ and $A^{4\sigma}$ in (A.3), we will not immediately make use of

(A.6). The reason for this is that a number of the terms cancel exactly, leading to simpler equations. For the amplitude equation, (A.3), we obtain

$$\underbrace{\frac{A''}{A} - \frac{b^2}{a^2\xi^2} - \frac{1}{a^2\xi^2} + \frac{1}{a\xi}A^{2\sigma}}_{\mathrm{O}(\xi^{-2})} - a\xi\gamma(\xi) = \mathrm{O}(\xi^{-3}). \tag{A.7}$$

One can check that the indicated terms are of order ξ^{-2}. Since we have assumed that $\gamma(\xi) = \mathrm{O}(\xi^{-3})$, $a\xi\gamma(\xi)$ will be $\mathrm{O}(\xi^{-2})$, and thus it is consistent. We could obtain the leading order ξ^{-3} term in γ, but we do not pursue this. The right-hand-side of (A.7) contains a number of terms that can be checked to be of order at least ξ^{-3}.

Turning to (A.4), we will explicitly retain all terms of order ξ^{-2}, and verify that $\nu(\xi)$ appears at the correct order. We first expand A_ξ/A using (A.6), to obtain

$$\frac{A_\xi}{A} = -\frac{1}{2\sigma\xi} - \frac{b}{2a\sigma\xi^2} + \frac{b^2}{4a^2\sigma^2\xi^3} + \nu_\xi(\xi) + \mathrm{O}(\xi^{-4}).$$

Under our assumption on ν, ν_ξ is of order ξ^{-3}. Then, substituting in the above expression into (A.4)

$$\underbrace{\frac{1}{a\xi^2} + \frac{b^2}{4a\sigma^2\xi^2} + \frac{1}{a\sigma\xi^2} + \frac{b^2}{2a\sigma\xi^2} - \frac{1}{2\sigma\xi}A^{2\sigma}}_{\mathrm{O}(\xi^{-2})} + a\xi\nu_\xi(\xi) = \mathrm{O}(\xi^{-3}). \tag{A.8}$$

The indicated terms on the left-hand-side of (A.8) are all of order ξ^{-2}. Under the assumption on ν and its derivatives, $a\xi\nu_\xi(\xi)$ is also $\mathrm{O}(\xi^{-2})$. Thus, we have a consistent expansion, and the leading order ξ^{-2} term in $\nu(\xi)$ could be obtained if needed. Again, one can check that the omitted terms in the expansion are all $\mathrm{O}(\xi^{-3})$, and have been put on the right-hand-side of this last equation. Returning to the Q variable, we have (2.6):

$$Q \approx A_\pm |\xi|^{\frac{-1}{2\sigma}} \left(1 + \frac{b}{2\sigma a\xi}\right) \exp\left\{\frac{-i}{a}\ln|\xi| + \frac{ib}{a^2\xi}\right\},$$

and the corrections in the phase and amplitude are at $\mathrm{O}(\xi^{-2})$.

Appendix B. Details of the Numerical Methods

Here, we report details of our numerical scheme for solving (1.10).

B.1. **Far Field Boundary Conditions.** To numerically solve (1.10), we restrict to the domain $[-\xi_{\max}, \xi_{\max}]$, and impose approximate boundary conditions at $\pm\xi_{\max}$. For $\xi_{\max}$ large enough, Q is approximated by (2.6) (see Proposition 2.3). This allows us to write linear Robin conditions. Writing Q in terms of its amplitude and phase, $Q = Ae^{i\phi}$, and also in terms of its real and imaginary parts $Q = u + iv$. Then

$$\phi_\xi = \frac{-vu_\xi + uv_\xi}{u^2 + v^2}, \quad A_\xi = \frac{uu_\xi + vv_\xi}{\sqrt{u^2 + v^2}}. \tag{B.1}$$

Using (2.6), we have that, as $\xi \to \pm\infty$,

$$\phi_\xi \approx -\frac{1}{a\xi} - \frac{b}{a^2\xi^2}, \quad \frac{A_\xi}{A} \approx -\frac{1}{2\sigma\xi} - \frac{b}{2a\sigma\xi^2}. \tag{B.2}$$

Defining $\alpha(\xi) \equiv \frac{1}{2\sigma\xi} + \frac{b}{2a\sigma\xi^2}$, $\beta(\xi) \equiv \frac{1}{a\xi} + \frac{b}{a^2\xi^2}$ and substituting in (B.1) we obtain for large $|\xi|$,

$$u_\xi + \alpha(\xi)u - \beta(\xi)v \approx 0, \quad v_\xi + \beta(\xi)u + \alpha(\xi)v \approx 0, \tag{B.3}$$

and thus the boundary conditions at $\pm\xi_{\max}$.

B.2. **Rescaling of the domain.** As seen in Section 3.3, the turning points of (1.10) are located at $\xi_- = -\epsilon/a$ and $\xi_+ = (4-\epsilon)/a$. In order to be in the asymptotically linear regime where (B.3) is valid, we need $\xi_{\max}$ to exceed $|\xi_\pm|$. This presents a problem numerically, since $\xi_\pm \to \pm\infty$, as $\sigma \to 1$. We thus rescale the domain, so that the turning points, in the rescaled coordinate system remain in a fixed domain. Setting $x = a\xi$, (1.10) becomes

$$a^2 Q_{xx} - Q + ia\left(\tfrac{1}{2\sigma}Q + xQ_x\right) - iabQ_x + ia\,|Q|^{2\sigma}\,Q_x = 0 \tag{B.4}$$

and boundary conditions (B.3), evaluated at $x_{\max}$, are

$$0 = u_x + \alpha(x)u - \beta(x)v, \quad 0 = v_x + \beta(x)u + \alpha(x)v, \tag{B.5}$$

with $\alpha(x) \equiv \frac{1}{2\sigma x} + \frac{b}{2\sigma x^2}$, $\beta(x) \equiv \frac{1}{ax} + \frac{b}{ax^2}$. In these coordinates, the turning points are at $x_- = -\epsilon$ and $x_+ = 4-\epsilon$. Eq. (B.4) is singular as $\sigma \to 1$ since $a \to 0$. However, we find this to be more effective, as it allows us to compute on a domain of fixed size for all values of σ.

B.3. **Numerical Implementation of the Boundary Value Problem.** We solve for Q using the default Newton solver in [3,4], along with a sparse direct linear solver. Due to the condition that the maximum of the profile occurs at the origin, an interior point of $(-x_{\max}, x_{\max})$, we introduce the variable $W(x) = Q(-x)$, and study Q and W on $(0, x_{\max})$, with Q and W coupled by a continuity condition at the origin. W then solves the equation

$$a^2 W_{xx} - W + ia\left(\tfrac{1}{2\sigma}W + xW_x\right) + iabW_x - ia\,|W|^{2\sigma}\,W_x = 0. \tag{B.6}$$

Setting $W = f + ig$, the boundary conditions (B.5) are

$$\begin{aligned} 0 &= -f_x + \alpha(-x_{\max})f - \beta(-x_{\max})g, \\ 0 &= -g_x + \beta(-x_{\max})f + \alpha(-x_{\max})g. \end{aligned}$$

We now solve these equations on a uniform mesh of $N+1$ mesh points on $[0, x_{\max}]$ to obtain $(u_j, v_j, f_j, g_j)_{j=0}^N$ along with a and b. First and second derivatives are approximated by second order centered finite differences. For instance, the real part of (B.4) becomes

$$\begin{aligned} &\tfrac{a^2}{\Delta x^2}\left(u_{j+1} - 2u_j + u_{j-1}\right) - u_j \\ &\quad + a\left(\tfrac{1}{2\sigma}v_j + (x_j - b + (u_j^2 + v_j^2)^\sigma)\tfrac{1}{2\Delta x}(v_{j+1} - v_{j-1})\right) = 0 \end{aligned} \tag{B.7}$$

After an analogous discretization, the farfield boundary conditions provide the needed values of $(u_{N+1}, v_{N+1}, f_{N+1}, g_{N+1})$ for evaluating equations like (B.7) at $j = N$.

In addition to the farfield conditions, we impose symmetry and anti-symmetry conditions at the origin,

$$u_{-1} = u_1, \quad v_{-1} = g_1, \quad f_{-1} = f_1, \quad g_{-1} = v_1$$

the auxiliary continuity conditions at the origin,

$$u_0 = f_0, \quad v_0 = g_0,$$

and the zero phase condition, $v_0 = 0$.

This system of $4 \times (N + 1) + 2$ unknowns is then solved with $x_{\max} = 25$. Solutions with $N = 1.28 \times 10^6, 2.56 \times 10^6, 5.12 \times 10^6$, were obtained. As a convergence criterion, we sought to ensure that we had good pointwise relative error, terminating when

$$|u_0 - f_0| \leq \text{TOL}, \quad |v_0 - g_0| \leq \text{TOL}, \frac{|(\text{B.7})|}{|u_j + iv_j|} \leq \text{TOL}, \tag{B.8}$$

and an analogous equation for the imaginary counterpart to (B.7), along with the f_j and g_j equations. We solved with $\text{TOL} = 10^{-6}$. We compared our results against those obtained using `BVP_SOLVER-2`, a successor to `BVP_SOLVER`, [5,19]. They were found to be in agreement, but we found that `BVP_SOLVER-2` was unable to solve for values of σ below 1.07, motivating us to switch algorithms.

B.4. **Continuation method.** As is the case for all Newton solvers, it is essential to provide a good initial guess. We use the solution obtained from the time integration of gDNLS $\sigma = 2$, and perform a continuation in σ, to solve for Q at smaller values. The initial guess for $\sigma = 2$ was constructed using the dynamic rescaling, [12]. Next, we construct a decreasing sequence of values of σ, $2 = \sigma_0 > \sigma_1 > \ldots > \sigma_j > \ldots$, using the solution at σ_{j-1} as the starting guess for solving the solution at σ_j. Starting with $\Delta\sigma = 0.2$, we reduce σ by $\Delta\sigma$, halving the size of $\Delta\sigma$ when the Newton solver fails. Below $\sigma = 1.1$, the largest value of $\Delta\sigma = 0.0125$, and for values close to the smallest resported value of $\sigma = 1.044$, $\Delta\sigma = 0.00078125$.

B.5. **Richardson Extrapolation.** Since this discretization is second order, we contend that quantities such as a and b should be $\mathrm{O}(\Delta x^2)$. Thus, we improve upon our results at different resolutions via Richardson extrapolation, *i.e.*, $a^{\text{Rich.}}(\sigma) = \frac{4}{3}a^{\Delta x/2}(\sigma) - \frac{1}{3}a^{\Delta x}(\sigma)$. This requires having values of the desired quantities available at the same values of σ. We use cubic spline interpolation to obtain values on common σ values.

B.6. **Limitations.** One limitation we found to our numerical calculations is due to the singular nature of the equation. Recall that we expect $a \to 0$ as $\sigma \to 1$. Since a corresponds to a length scale in (B.4), we should have $\Delta x \ll a$. Thus, as σ tends to 1 and a tends to zero, a consistent numerical

discretization requires ever smaller values of Δx. This limited us to values of σ near 1.04. Also, as shown in Figure 5, computed values of Q, in the tail, are reaching the limit of double precision floating point, as the values are smaller than 10^{-300}.

References

[1] David M Ambrose and Gideon Simpson. Local existence theory for derivative nonlinear Schrödinger equations with noninteger power nonlinearities. *SIAM Journal on Mathematical Analysis*, 47(3):2241–2264, 2015.

[2] D. Anderson and M. Lisak. Nonlinear asymmetric self-phase modulation and self-steepening of pulses in long optical waveguides. *Phys. Rev. A*, 27(3):1393–1398, 1983.

[3] S. Balay, S. Abhyankar, M.F. Adams, J. Brown, P. Brune, K. Buschelman, L. Dalcin, V. Eijkhout, W.D. Gropp, D. Kaushik, M.G. Knepley, L. Curfman McInnes, K. Rupp, B.F. Smith, S. Zampini, and H. Zhang. PETSc Web page. `http://www.mcs.anl.gov/petsc`, 2015.

[4] S. Balay, W. D. Gropp, L. Curfman McInnes, and B. F. Smith. Efficient management of parallelism in object oriented numerical software libraries. In E. Arge, A. M. Bruaset, and H. P. Langtangen, editors, *Modern Software Tools in Scientific Computing*, pages 163–202. Birkhäuser Press, 1997.

[5] J. J. Boisvert, P. H. Muir, and R. J. Spiteri. A numerical study of global error and defect control schemes for bvodes. Technical Report, `http://cs.stmarys.ca/~muir/BVP_SOLVER_Webpage.shtml`, 2012.

[6] C. J. Budd, S. Chen, and R. Russell. New self-similar solutions of the nonlinear Schrödinger equation with moving mesh computations. *J. Comput. Phys.*, 152(2):756–789, 1999.

[7] Masayuki Hayashi and Tohru Ozawa. Well-posedness for a generalized derivative nonlinear Schrödinger equation. arXiv:1601.04167, 2016.

[8] N. Hayashi. The initial value problem for the derivative nonlinear Schrödinger equation in the energy space. *Nonlinear Analysis. Theory, Methods & Apllications*, 20(7):823–833, 1993.

[9] N. Hayashi and T. Ozawa. On the derivative nonlinear Schrödinger equation. *Physica D: Nonlinear Phenomena*, 55(1-2):14–36, 1992.

[10] D.J. Kaup and A. C Newell. An exact solution for a derivative nonlinear Schrödinger equation. *J. Math. Phys.*, 19(4):798–801, 1978.

[11] J. Liu, P. Perry, and C. Sulem. Global Existence for the Derivative Nonlinear Schrödinger Equation by the Method of Inverse Scattering. arXiv:1511.01173, 2015.

[12] X. Liu, G. Simpson, and C. Sulem. Focusing singularity in a derivative nonlinear Schrödinger equation. *Physica D*, 262:48–58, 2013.

[13] X. Liu, G. Simpson, and C. Sulem. Stability of Solitary Waves for a Generalized Derivative Nonlinear Schrödinger Equation. *J. Nonlinear Sci.*, 23(4):557–583, 2013.

[14] D.W. McLaughlin, G.C. Papanicolaou, C. Sulem, and P.-L. Sulem. The focusing singularity of the cubic schrödinger equation. *Phys. Rev. A*, 34:1200–1210, 1986.

[15] F. Merle, P. Raphaël, and J. Szeftel. Stable self similar blow up for slightly l^2 supercritical nls equations. *Geom. Funct. Anal.*, 20(4):1028–1071, 2010.

[16] J. Moses, B. A. Malomed, and F. W. Wise. Self-steepening of ultrashort optical pulses without self-phase-modulation. *Phys. Rev. A*, 76(2), 2007.

[17] D. Pelinovsky and Y. Shimabukuro. Existence of global solutions to the derivative NLS equation with the inverse scattering transform method. Preprint, 2015.

[18] G. Sanchez-Arriaga, D. Laveder, T. Passot, and P.-L. Sulem. Quasicollapse of oblique solitons of the weakly dissipative derivative nonlinear Schrodinger equation. *Phys. Rev. E*, 82(1):016406, 2010.

[19] L. F. Shampline, P. H. Muir, and H. Xu. A user-friendly fortran bvp solver. *JNAIAM*, 1(2):201–217, 2006.
[20] C. Sulem and P.-L. Sulem. *The Nonlinear Schrödinger Equation: Self-Focusing and Wave Collapse*. Springer, 1999.
[21] N. Tzoar and M. Jain. Self-phase modulation in long-geometry optical waveguides. *Phys. Rev. A*, 23(3):1266–1270, 1981.
[22] Y. Wu. Global well-posedness on the derivative nonlinear Schrödinger equation revisited. *arxiv.org 1404.5159v3*, April 2014.

Department of Mathematics, University of Toronto, Toronto ON, M5S 2E4 Canada, ycher@math.toronto.edu

Department of Mathematics, Drexel Unixersity, Philadelphia PA, 19104, simpson@math.drexel.edu

Department of Mathematics, University of Toronto, Toronto ON, M5S 2E4 Canada, sulem@math.toronto.edu